Electronic Supporting Information

A two-enzyme cascade reaction consisting of two reaction pathways. Studies in bulk solution for understanding the performance of a flow-through device with immobilised enzymes.

Nicolas Ghéczy,[a,±] Kai Sasaki,[a,1,±] Makoto Yoshimoto,[a,b] Sajad Pour-Esmaeil,[a,2] Martin Kröger,[c] Pasquale Stano,[d] Peter Walde[a]*

[a] Laboratory for Multifunctional Materials, Department of Materials, ETH Zürich, Vladimir-Prelog-Weg 5, CH-8093 Zürich, Switzerland

[b] Department of Applied Chemistry, Yamaguchi University, Tokiwadai 2-16-1, Ube 755-8611, Japan

[c] Polymer Physics, Department of Materials, ETH Zürich, Leopold-Ruzicka-Weg 4, CH-8093 Zürich, Switzerland

[d] Department of Biological and Environmental Sciences and Technologies (DiSTeBA), University of Salento, Ecotekne, 73100 Lecce, Italy

[1] Current affiliation: Graduate School of Organic Materials Science, Yamagata University, Yonezawa, 4-3-16 Jonan, Yonezawa, Yamagata, 9992-8510, Japan

[2] Current affiliation: Polymer Laboratory, Nano-Chemistry Division, School of Chemistry, College of Science, University of Tehran, P.O. Box 14155-6455, Tehran, Iran

[±] Equal contributions

Content

1. Acid-base equilibria of DCFH$_2$, DCFH$^\bullet$, and DCF
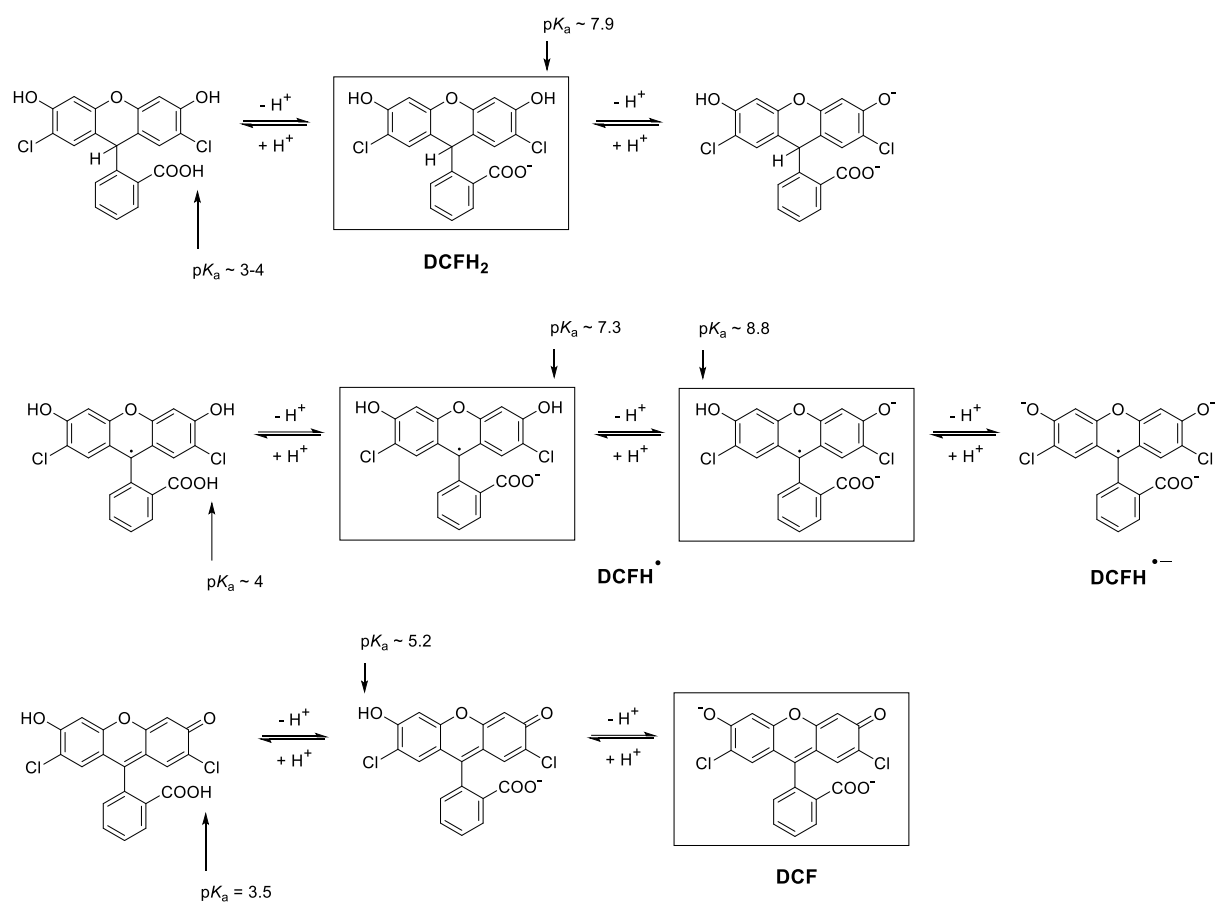
Figure S-1. Some of the relevant acid-base equilibria for DCFH$_2$, DCFH$^\bullet$, and DCF. For pH = 7.2 conditions, the most abundant species are marked with a frame. Relevant pK_a values are indicated, as determined by (Wrona and Warman, 2006).[S1]

2. Chemical structures of different fluorescein derivatives
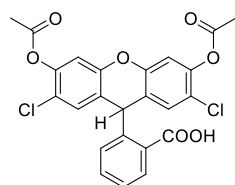
DCFH₂-DA
2',7'-dichlorodihydrofluorescein diacetate
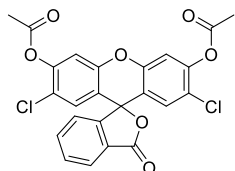
DCF-DA
2'-7'-dichlorofluorescein diacetate
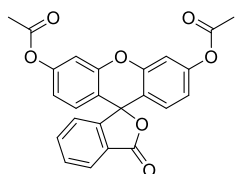
fluorescein diacetate
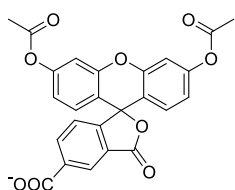
6-carboxyfluorescein diacetate

Figure S-2. Comparison of the chemical structures of DCFH₂-DA (2',7'-dichlorodihydrofluorescein diacetate), 2'-7'-dichlorofluorescein diacetate, fluorescein diacetate, and 6-carboxyfluorescein diacetate.

3. Absorption spectra of DCF
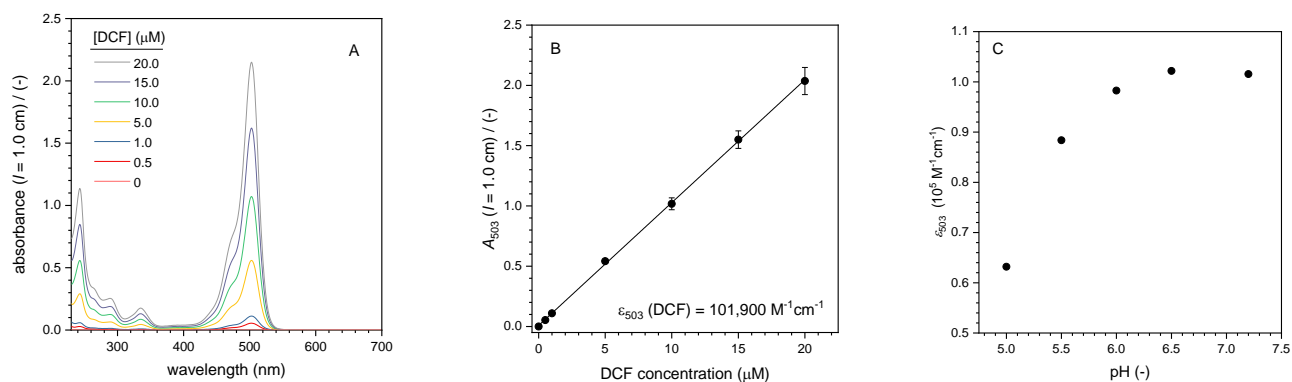
Figure S-3. Concentration dependence of the absorption spectrum of DCF dissolved in PB (10 mM sodium phosphate buffer solution, pH = 7.2). **(A)** Spectra for [DCF] = 0, 0.5, 1.0, 5.0, 10.0, 15.0, and 20.0 μM, path length l = 1.0 cm, T = 25 °C. **(B)** A_{503} vs. [DCF], plotted as mean values ± standard deviations (n = 3, separately prepared solutions from three different DCF stock solutions). The molar absorption coefficient for λ = 503 nm was determined, ε_{503} (DCF) = $1.02 \cdot 10^5$ M^{-1}cm^{-1}. **(C)** Dependence of the molar absorption coefficient at λ = 503 nm, ε_{503} (DCF), on pH.

4. Details about the preparation of *de*-PG2$_{1000}$-BAH-enzyme conjugates

4.1. Conjugates *de*-PG2$_{1000}$-BAH$_{152}$-BCA$_{101}$ and *de*-PG2$_{1000}$-BAH$_{207}$-BCA$_{152}$

The denpol-enzyme conjugates *de*-PG2$_{1000}$-BAH$_{152}$-BCA$_{101}$ and *de*-PG2$_{1000}$-BAH$_{207}$-BCA$_{152}$ were

obtained in a similar way as described before for the preparation of *de*-PG2$_{1000}$-BAH$_{175}$-BCA$_{115}$, see

(Yoshimoto et al., 2018).[S2] Besides, there were small experimental variations (slightly higher amounts

of BAH formed during the conjugation reaction as compared to the amounts of added 4FB; [4FB]

being determined by spectral fitting). All materials used were the same as before,[S2] except *de*-PG$_{1000}$;

it was the same as the one used in the work of (Hou et al., 2019).[S3] For the spectral changes during

conjugate formation, see **Figure S-4**. For comparison, some of the characteristic data for the

conjugate formation are provided:

de-PG2$_{1000}$-BAH$_{175}$-BCA$_{115}$ (Yoshimoto et al., 2018): [S2]

- MSR (4FB/BCA) = 1.02
- *de*-PG2$_{1000}$-HyNic$_{440}$
- used for conjugation reaction: [4FB] = 67 µM, [HyNic] = 120 µM, pH = 7.2
- observed in conjugation reaction: [BAH] = 48 µM
- [BCA]/[BAH] in conjugate = 0.66 (66 %)

de-PG2$_{1000}$-BAH$_{152}$-BCA$_{101}$ (this work, used for measurement with *p*-NA in a BCA loaded glass fiber filter only):

- MSR (4FB/BCA) = 0.99
- *de*-PG2$_{1000}$-HyNic$_{436}$
- used for conjugation reaction: [4FB] = 37 µM, [HyNic] = 120 µM, pH = 7.2
- observed in conjugation reaction: [BAH] = 42 µM
- [BCA]/[BAH] in conjugate = 0.66 (66 %)

de-PG2$_{1000}$-BAH$_{207}$-BCA$_{152}$ (this work, used for the cascade reaction in the glass fiber filter flow-through device):

- MSR (4FB/BCA) = 0.84
- *de*-PG2$_{1000}$-HyNic$_{362}$
- used for conjugation reaction: [4FB] = 60 µM, [HyNic] = 120 µM, pH = 7.2
- observed in conjugation reaction: [BAH] = 68 µM
- [BCA]/[BAH] in conjugate = 0.73 (73 %)
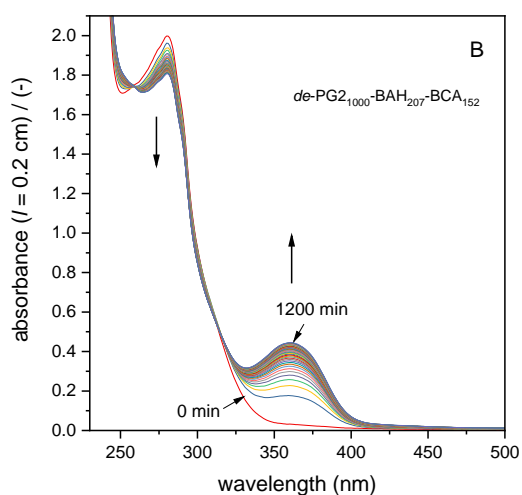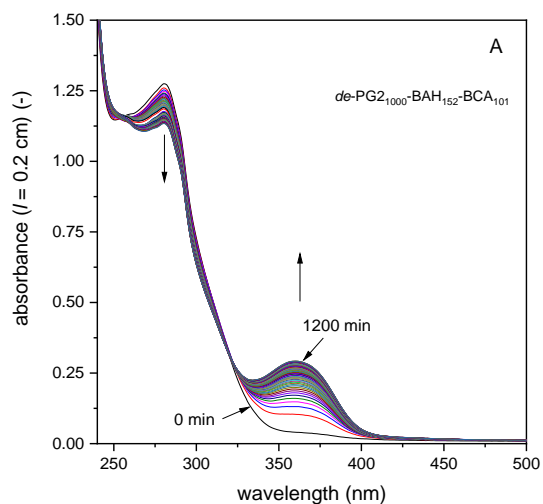
Figure S-4. Conjugation reaction between **(A)** *de*-PG2$_{1000}$-HyNic$_{436}$ and BCA-4FB (MSR(4FB/BCA) = 0.99), and **(B)** *de*-PG2$_{1000}$-HyNic$_{362}$ and BCA-4FB (MSR(4FB/BCA) = 0.84). The absorption spectrum was recorded every 30 min during a total reaction time of 20 h (reaction between HyNic and 4FB to form stable BAH (bis-aryl hydrazone) bonds between the denpol and BCA). The absorption band of the BAH bond formation (centered around λ = 354 nm) as well as a decrease in band intensity around λ = 280 nm (HyNic and 4FB) are visible and indicate the ongoing conjugation reaction.

From A_{354}(20 h) - A_{354}(0 h), the concentration of BAH formed could be calculated. With the known amounts of added denpol r.u. and BCA (as well the free, unbound BCA recovered from the reaction mixture during purification), the ratio of BAH to BCA in the conjugate could be estimated to *de*-PG2$_{1000}$-BAH$_{152}$-BCA$_{101}$ **(A)** and *de*-PG2$_{1000}$-BAH$_{207}$-BCA$_{152}$ **(B)**.

4.2. Conjugate de-PG2$_{1000}$-BAH$_{86}$-HRP$_{90}$

The denpol-enzyme conjugate de-PG2$_{1000}$-BAH$_{86}$-HRP$_{90}$ was obtained in a similar way as described

before for the preparation of de-PG2$_{1000}$-BAH-HRP$_{71}$, see (Hou et al., 2019).[S3] This time, the pH value

of the conjugation reaction buffer used was a bit lower: pH = 4.4 instead of 4.7, noted as "*MesB1*" in

(Hou et al., 2019).[S3] This deviation did not lead to significant changes in the conjugation reaction. The

filtrates obtained during purification of the conjugate solution by ultrafiltration were quantified for

HRP content by measuring the heme group absorption at A_{403}. Assuming that non-conjugated HRP

could pass the ultrafiltration membrane quantitatively (100 kDa MWCO), the total amount of HRP in

the ultrafiltrate was determined and subtracted from the total amount of HRP used for the

conjugation reaction. In this way, the amount of conjugated HRP was determined and compared with

the amount of BAH bonds formed (subscripts of HRP and BAH, respectively). With this, the previously

made assumption that for each BAH bond formed about one HRP molecule is conjugated, see (Hou

et al., 2019),[S3] could be confirmed (86 BAH and 90 HRP per 1000 r.u.). The higher amount of

conjugated HRP (and BAH bonds) per 1000 r.u. – around 90 per average denpol chain in this work,

around 70 previously[S3] – can be explained by the higher content of HyNic in the denpol used in this

work (de-PG2$_{1000}$-HyNic$_{310}$) as compared to the one in our previous work (de-PG2$_{1000}$-HyNic$_{240}$).[S3] In

both denpol-HRP conjugate reactions, the same concentrations of HyNic and 4FB were used, leading

to similar extent of BAH bond formation, while the concentration of r.u. during the conjugation

reaction was lower in the work presented, as compared to the previous preparation. All materials

used were the same as in (Hou et al., 2019).[S3] For the spectral changes during conjugate formation,

see **Figure S-5**. For comparison, some of the characteristic data for the conjugate formation are

provided:

de-PG2$_{1000}$-BAH-HRP$_{71}$ (Hou et al., 2019):[S3]

- MSR (4FB/HRP) = 0.73
- de-PG2$_{1000}$-HyNic$_{240}$
- used for conjugation reaction: [4FB] = 50 µM, [HyNic] = 100 µM, pH = 4.7
- observed in conjugation reaction: [BAH] = 29.5 µM
- [HRP]/[BAH] in conjugate assumed to be 1:1 as MSR(4FB/HRP) < 1.

8

de-PG2$_{1000}$-BAH$_{86}$-HRP$_{90}$ (this work):

- MSR (4FB/HRP) = 0.62
- *de*-PG2$_{1000}$-HyNic$_{310}$
- used for conjugation reaction: [4FB] = 50 µM, [HyNic] = 100 µM, pH = 4.4
- observed in conjugation reaction: [BAH] = 27.9 µM
- [HRP]/[BAH] in conjugate = 1.05 (105 %) (slight excess, experimentally determined)
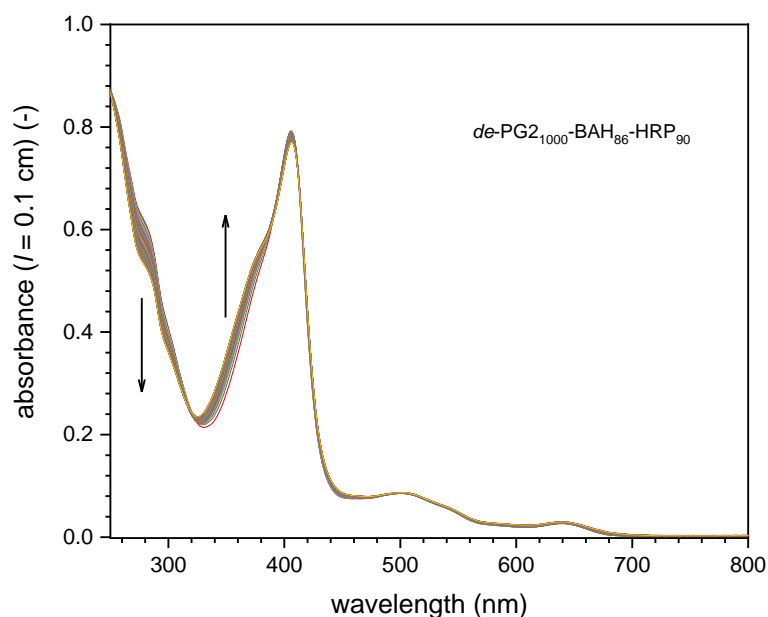
Figure S-5. Conjugation reaction between *de*-PG2$_{1000}$-HyNic$_{310}$ and HRP-4FB (MSR(4FB/HRP) = 0.62). The absorption spectrum was recorded every 30 min during a total reaction time of 20 h (reaction between HyNic and 4FB to form stable BAH (bis-aryl hydrazone) bonds between the denpol and HRP). The absorption band of the BAH bond formation (centered around λ = 354 nm) as well as a decrease in band intensity around λ = 280 nm (HyNic and 4FB) are visible and indicate the ongoing conjugation reaction. The strong band at λ = 403 nm is due to the heme group of HRP.

From A_{354}(20 h) - A_{354}(0 h), the concentration of BAH formed could be calculated. With the known amounts of added denpol r.u. and HRP (as well the free, unbound HRP recovered from the reaction mixture during purification), the ratio of BAH to HRP in the conjugate could be estimated to *de*-PG2$_{1000}$-BAH$_{86}$-HRP$_{90}$.

5. Details about deviations from the general procedure applied for the immobilisation of denpol-enzyme conjugates in glass fiber filters

Compared to the general procedure described in section 2.5. for the immobilisation of denpol-enzyme conjugates in glass fiber filters, there were a few variations, as indicated below.

Deviations in experiment ① (see **Figure 11**): One of the two independent experiments using sequentially- and co-immobilized denpol-BCA and denpol-HRP loaded filters for activity measurements with $DCFH_2$-DA and H_2O_2 (see **Figure 12**, triangles, "exp. 1"). Instead of keeping the incubation buffer fixed for sequential and co-immobilization (as used for "exp. 2", 80% PB, 20% of 10mM phosphate, pH 7.0, 0.15 M NaCl, see 2.5.2 and 2.5.3), for the sequential immobilization each denpol-enzyme was incubated with the same buffer as for the individual incubations of one filter per holder (no NaCl in the BCA-denpol incubation buffer, see 2.5.1). In case of the co-immobilisation, a buffer ratio was used as close to PB as the denpol-HRP stock solution (in other buffer) allowed (finally 88.5% PB, 11.5% of 10mM phosphate, pH 7.0, 0.15 M NaCl). By that slight variation within "exp. 1" and "exp. 2" it could be checked if the NaCl contained in the buffer used for immobilization of BCA-conjugate in this work (in contrast to the NaCl-less incubation buffer, as introduced in (Yoshimoto et al. 2018))[S2] had any influence on the cascade experiment. From the results obtained (**Figure 12** and **Figure S-21**, comparison of **Figure 13** and **Figure S-22**), no significant change upon buffer modification was visible.

Deviations in experiment ② (see **Figure 11**): single denpol-BCA loaded filter for activity measurements with *p*-NA (see **Figure 9**). The BCA-conjugate stock solution used was *de*-$PG2_{1000}$-BAH_{152}-BCA_{101} (instead of *de*-$PG2_{1000}$-BAH_{207}-BCA_{152}) and was diluted to [BAH] = 3.3 µM and [BCA] = 2.2 µM (instead of [BAH] = 12 µM and [BCA] = 8.8 µM) for the incubation. For the washing step, the filter containing the conjugate was immersed three times in 1.5 mL fresh PB for 15 min (instead of washing by pumping PB through the filter placed in the filter holder).

Deviations in experiment ③ (see **Figure 11**): single denpol-HRP loaded filters for activity measurements with $ABTS^{2-}/H_2O_2$ (see **Figure 10**). The filters were loaded with 50 or 250 µL of the conjugate solution. In the case of loading with 50 µL, after incubation for 1 h, the filter was washed for 5 h (instead of 3 h). For the loading with 250 µL, after incubation for 1 h, the filter was first washed by 8 times immersion in 1.5 mL fresh phosphate buffer solution (100 mM sodium phosphate, 1.15 M NaCl, pH = 7.2) and storage for 15 min. Afterwards, the filter was placed in the filter holder and washed by pumping the phosphate buffer solution though the filter for 3 h.

6. Details about the visualisation of the denpol-BAH-enzyme conjugates prepared

In an attempt to visualise the space occupied by enzymes bound onto the surface of the polymer (*de*-PG2), we represent the situation using a solid cylinder for a fraction carrying 100 r.u. of *de*-PG2, and identical, non-overlapping spheres for the proteins a variable distance (Δ) between 0 and 1 nm away from the polymer surface (see **Figure 1**, right). The conformation of 100 r.u. of PG2 can be considered cylindrical, as the contour length of its backbone does not exceed the persistence length of PG2, $\lambda^* \approx 25$ nm,[S4] and because the radial density profile of the polymer is known to exhibit a plateau at small distances before it decays beyond approximately 1.5 nm, see Figure 9 in (Bertran et al., 2013).[S5] The corresponding effective PG2 radius is in rough agreement with an estimate of 2.5 nm.[S4] We use this radius for the visualisation, assuming the deprotection of PG2 (thus *de*-PG2, without the Boc protection group from PG2) did not significantly change it. The volume of the spheres we choose to match the volume of the protein (BCA or HRP) using the empirical expression from Fischer et al., 2004)[S6] for the effective mass density ρ_p of proteins, $\rho_p \approx [1.41 + 0.145 \exp(-M_p /13)]$ g/cm^3, where M_p is the molecular mass of a protein in units of kDa. Using $M_p = 29$ for BCA (RCSB PDB: 1V9E) and $M_p = 44$ for HRP (RCSB PDB: 1HCH) the resulting sphere radii are $R_p = 2.0$ nm (BCA) and $R_p = 2.3$ nm (HRP). The distance Δ takes into account the linkers located between polymer and enzyme. Each BAH linker is modelled as a flexible trimer with two bonds of fixed length 0.5 nm, where the first bond is taken normal to the *de*-PG2 surface, and the second bond chosen randomly. The mean amount of bound enzymes per 100 r.u. is provided by our experimental values for 1000 r.u. *de*-PG2. The centers of the spheres are determined using a random number generator, that specifies a location on the surface of a cylinder with radius 2.5 nm + Δ + R_p and length λ^*. Attempted locations that lead to overlap between existing spheres are rejected, while non-overlapping spheres are accepted. Every visualised configuration is thus different (if repeated with same input values), but each of them is a representant of the ensemble.

7. UV/vis absorption spectra of BCA, HRP, DCFH$_2$-DA, DCFH$_2$-MA, DCFH$_2$, DCF-MA, DCF, and DCF$_{ox}$

Table S-1. Molar absorption coefficients ε_λ (M^{-1}cm^{-1}) for BCA (measured),[a] HRP (measured),[b] H$_2$O$_2$ (measured), DCFH$_2$-DA (measured), DCFH$_2$-MA (fitted), DCFH$_2$ (measured), DCF-MA (fitted), DCF (measured), and DCF$_{ox}$ (measured). PB (10 mM sodium phosphate, pH = 7.2), T = 25 °C. Wavelength range: λ = 240 - 600 nm.

[a]: ε_{280} (BCA) set to 5.6·10^4 (M^{-1}cm^{-1});[S7] and [b]: ε_{403} (HRP) set to 1.02·10^5 (M^{-1}cm^{-1}).[S8]

Please note that negative values for absorption coefficients given in the table have no physical meaning. They are mainly the result from measurement background/noise or spectral fitting where they reflect the background/noise of the actual measurements from which the spectra were fitted. The data in the table are the ones used for the actual quantitative analysis of the reaction mixtures (including the negligible, small negative values).

Wavelength (nm)	BCA (stock solution)	HRP (stock solution)	H$_2$O$_2$ (stock solution)	DCFH$_2$-DA (stock solution)	DCFH$_2$-MA (fitted)	DCFH$_2$ (prepared *in situ*)	DCF-MA (fitted)	DCF (stock solution)	DCF-fully oxidized (prepared *in situ*)
600	476	2340	0	-16	-17	-19	-96	-176	-81
599	463	2350	0	-17	-18	-17	-88	-173	-84
598	451	2330	0	-19	-16	-17	-110	-159	-85
597	460	2340	0	-17	-13	-13	-76	-145	-65
596	474	2390	0	-18	-36	-18	-56	-137	-75
595	472	2410	0	-16	-21	-14	-61	-142	-65
594	473	2410	0	-16	-23	-14	-74	-154	-53
593	465	2440	0	-19	-17	-15	-115	-155	-57
592	477	2460	0	-21	-19	-19	-115	-155	-48
591	490	2490	0	-18	-23	-15	-133	-157	-52
590	477	2530	0	-15	-22	-13	-140	-165	-47
589	462	2500	0	-15	-22	-13	-107	-163	-31
588	462	2530	0	-14	-24	-16	-107	-166	-37
587	458	2530	0	-14	-10	-14	-85	-174	-26
586	476	2560	0	-16	-8	-12	-54	-150	-16
585	473	2600	0	-15	-14	-13	-63	-148	-28
584	461	2640	0	-15	-13	-13	-80	-166	-16
583	474	2670	0	-16	-9	-12	-73	-150	-10
582	478	2690	0	-19	-23	-13	-98	-153	11
581	471	2720	0	-17	-14	-14	-103	-158	9
580	453	2740	0	-15	-23	-17	-110	-152	12
579	469	2790	0	-16	-24	-13	-110	-160	34
578	467	2830	0	-13	-21	-8	-87	-163	55
577	478	2880	0	-14	-23	-10	-41	-150	63
576	467	2870	0	-16	-18	-11	-27	-147	67
575	484	2960	0	-16	-18	-11	-48	-134	77
574	496	3020	0	-16	-22	-9	-52	-139	96
573	477	3070	0	-15	-19	-11	-81	-147	100
572	477	3120	0	-13	-11	-13	-75	-135	117
571	472	3190	0	-14	-16	-12	-75	-144	140
570	483	3270	0	-16	-22	-12	-83	-133	166
569	490	3320	0	-15	-14	-10	-101	-125	199
568	496	3430	0	-12	-13	-11	-87	-119	206
567	481	3500	0	-13	-21	-11	-60	-114	219
566	498	3660	0	-15	-10	-9	-59	-123	242
565	490	3710	0	-15	-3	-8	-72	-137	278
564	455	3810	0	-13	-11	-11	-93	-139	293
563	475	3920	0	-14	-15	-12	-92	-140	323
562	488	4090	0	-16	-29	-12	-73	-136	348

561	477	4210	0	-18	-19	-11	-49	-109	398
560	458	4310	0	-19	-17	-11	-59	-117	434
559	472	4510	0	-13	-21	-9	-55	-108	480
558	510	4740	0	-11	-7	-8	-60	-96	527
557	503	4860	0	-9	-7	-4	-58	-102	589
556	496	5070	0	-12	-14	-6	-55	-94	637
555	470	5210	0	-10	-18	-5	-66	-90	694
554	471	5390	0	-9	-18	-3	-91	-90	759
553	523	5650	0	-18	-17	-11	-82	-76	823
552	505	5730	0	-15	-28	-13	-67	-47	919
551	493	5910	0	-12	-12	-10	-62	-35	1010
550	476	6090	0	-15	-24	-8	-65	-22	1110
549	508	6300	0	-14	-13	-6	-75	2	1200
548	516	6480	0	-12	-4	-5	-42	28	1310
547	509	6620	0	-11	-13	-5	-37	70	1460
546	512	6810	0	-15	-9	-7	-27	117	1570
545	512	6980	0	-16	-6	-4	17	175	1720
544	488	7110	0	-13	-10	-1	-26	229	1900
543	492	7250	0	-10	-9	0	-55	290	2060
542	513	7420	0	-12	-5	3	-15	401	2250
541	511	7550	0	-13	-1	-1	-53	491	2450
540	514	7650	0	-14	-4	-1	-51	613	2650
539	515	7810	0	-9	-2	3	18	787	2900
538	494	7890	0	-15	-3	-1	-4	972	3130
537	509	8030	0	-13	-2	3	9	1210	3380
536	504	8150	0	-15	-7	2	15	1500	3660
535	504	8230	0	-8	4	12	-13	1840	3980
534	502	8350	0	-5	-7	8	-23	2230	4290
533	524	8510	0	-12	-8	7	-49	2710	4580
532	533	8650	0	-11	5	10	-57	3310	4920
531	530	8720	0	-11	13	11	-69	4030	5260
530	526	8860	0	-9	-1	13	-89	4890	5620
529	522	9020	0	-12	0	14	-93	5920	5980
528	510	9110	0	-11	6	18	-131	7120	6340
527	534	9260	0	-12	10	20	-201	8540	6710
526	547	9390	0	-12	24	24	-256	10180	7090
525	544	9560	0	-9	15	26	-320	12090	7480
524	521	9620	0	-9	18	31	-356	14330	7860
523	528	9770	0	-10	19	36	-406	16900	8250
522	535	9930	0	-7	10	35	-444	19850	8600
521	538	10060	0	-10	28	39	-432	23190	8980
520	532	10030	0	-9	42	47	-5	27040	9350
519	538	10190	0	-7	47	54	29	31240	9710
518	535	10330	0	-7	45	59	16	35830	10050
517	529	10510	0	-11	49	63	10	40780	10370
516	553	10640	0	-7	65	71	101	46080	10710
515	569	10770	0	-11	59	75	111	51680	11010
514	557	10900	0	-7	69	84	100	57500	11280
513	540	10950	0	-9	83	93	47	63450	11530
512	565	11070	0	-8	98	100	-73	69410	11770
511	554	11140	0	-8	102	106	-72	75270	12020
510	551	11230	0	-3	110	116	-189	80820	12200
509	564	11380	0	-6	111	116	-183	85970	12340
508	568	11440	0	-7	121	126	-126	90580	12440
507	572	11460	0	-1	123	135	-14	94540	12560
506	579	11510	0	-6	130	135	259	97710	12590
505	562	11570	0	-7	131	137	584	100020	12600
504	567	11620	0	-7	145	140	1020	101430	12560
503	564	11630	0	-1	142	143	1460	101900	12490
502	564	11670	0	-1	139	142	2090	101490	12390
501	564	11650	0	-6	141	136	2630	100230	12240
500	551	11670	0	-6	142	133	3340	98220	12070
499	563	11660	0	-6	133	131	4040	95570	11890
498	550	11640	0	-7	133	128	4840	92380	11720
497	571	11660	0	-1	122	120	5770	88800	11520
496	583	11660	0	-5	120	116	6510	84950	11270
495	569	11640	0	-6	110	111	7220	80900	11060
494	577	11610	0	-9	116	106	7960	76830	10830
493	575	11590	0	-9	104	98	8550	72750	10620
492	581	11560	0	-10	92	93	9190	68750	10430
491	582	11530	0	-8	79	88	9840	64930	10220
490	578	11510	0	-6	78	83	10400	61320	10020

489	566	11440	0	-4	86	80	10880	57930	9840
488	546	11360	0	-2	89	79	11330	54800	9670
487	574	11340	0	-1	90	78	11670	51930	9540
486	575	11260	0	2	81	73	12020	49340	9390
485	603	11200	0	-4	64	65	12350	47050	9230
484	608	11150	0	-2	67	64	12630	45040	9100
483	583	11080	0	-3	65	62	12900	43290	8990
482	591	11020	0	-3	58	63	13090	41790	8900
481	565	10890	0	-2	57	63	13290	40490	8810
480	561	10850	0	-2	60	58	13480	39390	8710
479	599	10870	0	-2	62	59	13720	38480	8650
478	614	10790	0	-5	65	59	13950	37690	8580
477	603	10710	0	-7	44	54	14190	36990	8500
476	590	10650	0	-2	56	55	14470	36360	8440
475	600	10580	0	-1	61	52	14740	35710	8370
474	600	10520	0	-3	50	49	15040	35090	8290
473	594	10510	0	-4	41	47	15400	34440	8230
472	616	10520	0	-7	40	46	15770	33700	8160
471	601	10480	0	-4	33	48	16140	32900	8060
470	618	10440	0	-5	37	45	16520	32030	8000
469	624	10430	0	0	44	50	16930	31030	7920
468	607	10360	0	-3	45	47	17400	29990	7830
467	626	10410	0	-7	23	41	17860	28860	7720
466	626	10420	0	0	36	42	18250	27610	7630
465	630	10360	0	-3	26	39	18680	26350	7490
464	620	10350	0	-2	45	36	19070	25040	7380
463	635	10390	0	-4	42	34	19460	23710	7260
462	623	10350	0	-1	28	32	19820	22390	7130
461	665	10370	0	-2	14	28	20040	21050	7010
460	658	10340	0	-1	24	31	20190	19760	6880
459	655	10340	0	-2	14	28	20360	18500	6740
458	642	10350	0	0	16	28	20560	17320	6600
457	649	10330	0	4	16	30	20630	16200	6480
456	658	10300	0	-1	17	25	20610	15130	6320
455	627	10280	0	-4	10	19	20520	14150	6200
454	653	10340	0	0	8	14	20380	13250	6090
453	637	10270	0	-1	10	18	20240	12410	5950
452	652	10320	0	-3	9	16	20060	11670	5820
451	676	10380	0	-3	11	17	19790	10970	5730
450	650	10440	0	-2	6	19	19530	10350	5630
449	655	10540	0	0	12	17	19290	9810	5540
448	674	10660	0	-1	7	15	19020	9290	5440
447	652	10740	0	-2	4	12	18810	8850	5380
446	651	10900	0	-1	7	13	18500	8420	5290
445	685	11190	0	1	7	10	18250	8020	5230
444	693	11430	0	0	4	13	18040	7660	5180
443	663	11660	0	-6	1	15	17770	7290	5080
442	665	12000	0	0	7	13	17630	6960	5020
441	695	12470	0	5	1	14	17510	6640	5000
440	677	12870	0	0	-11	12	17390	6320	4930
439	671	13400	0	-1	-21	8	17280	6010	4840
438	704	14040	0	1	-5	10	17150	5690	4800
437	705	14750	0	-1	0	13	16990	5380	4750
436	687	15470	0	-3	-2	8	16820	5070	4680
435	702	16280	0	-1	0	12	16680	4790	4630
434	668	17210	0	-4	1	11	16570	4530	4540
433	658	18250	0	-1	-1	10	16410	4260	4480
432	710	19490	0	-1	5	8	16300	4000	4410
431	677	20750	0	-3	6	5	16170	3750	4340
430	693	22230	0	1	14	8	15940	3530	4260
429	713	23920	0	2	16	10	15740	3340	4180
428	727	25730	0	3	-2	12	15440	3150	4110
427	741	27670	0	0	-2	11	15120	2960	4030
426	754	29880	0	0	-3	6	14810	2790	3950
425	742	32190	0	-1	-18	4	14460	2600	3860
424	723	34700	0	2	-10	5	14140	2460	3780
423	729	37570	0	3	-1	7	13860	2370	3710
422	752	40560	0	1	-9	9	13570	2280	3660
421	726	43700	0	7	6	8	13290	2210	3580
420	829	47430	0	5	9	4	12980	2110	3490
419	837	51020	0	7	9	14	12720	2040	3460
418	809	54840	0	6	-13	8	12480	1970	3400

417	766	58890	0	0	-30	2	12260	1920	3340
416	799	63180	0	2	-17	4	12100	1880	3280
415	819	67530	0	10	-16	8	11990	1850	3220
414	852	71980	0	0	-10	2	11850	1840	3170
413	823	76370	0	-7	5	-1	11720	1810	3120
412	850	80700	0	-3	4	4	11640	1760	3070
411	875	84830	0	0	-17	3	11590	1730	3020
410	892	88630	0	0	1	5	11590	1700	2970
409	903	92110	0	2	-16	0	11660	1670	2970
408	912	95050	0	0	-15	1	11720	1660	2910
407	911	97480	0	-1	-16	3	11790	1660	2910
406	904	99340	0	0	-5	0	11930	1640	2880
405	873	100770	0	2	-14	3	12000	1620	2880
404	893	101560	0	1	-6	4	12160	1600	2870
403	896	101980	0	7	-17	12	12290	1590	2900
402	949	101930	0	5	-3	9	12380	1570	2920
401	965	101270	0	-2	-7	4	12550	1580	2930
400	918	100330	0	-2	5	4	12630	1570	2910
399	917	99240	0	6	-2	8	12760	1550	2960
398	903	97920	0	5	8	15	12860	1540	3000
397	909	96330	0	2	-1	13	12970	1540	3010
396	877	94690	0	7	-24	8	13050	1560	3040
395	919	93190	0	5	-25	2	13130	1570	3040
394	908	91570	0	4	-25	4	13270	1580	3060
393	949	89980	0	5	-7	8	13320	1560	3120
392	953	88410	0	5	-14	11	13430	1540	3150
391	955	87040	0	3	-13	11	13570	1540	3150
390	966	85630	0	2	9	11	13640	1540	3190
389	982	84270	0	8	-9	15	13730	1540	3200
388	937	82980	0	7	-13	11	13790	1530	3210
387	908	81820	0	7	-1	8	13870	1520	3270
386	951	80760	0	4	-21	6	13950	1500	3240
385	982	79610	0	9	-1	9	14060	1490	3290
384	947	78550	0	8	-14	4	14130	1490	3290
383	935	77490	0	3	-9	3	14190	1470	3300
382	948	76380	0	5	-2	3	14270	1440	3320
381	973	75350	0	11	0	7	14310	1420	3340
380	953	74140	0	7	2	8	14390	1370	3340
379	978	72950	0	7	9	12	14440	1350	3390
378	1010	71780	0	-1	13	11	14470	1340	3410
377	941	70400	0	-3	-5	7	14530	1330	3430
376	933	68970	0	-1	-10	-3	14580	1310	3390
375	948	67520	0	11	-5	5	14590	1270	3450
374	962	66030	0	4	-18	10	14550	1220	3480
373	950	64400	0	12	-7	12	14510	1200	3510
372	958	62870	0	14	5	15	14460	1200	3560
371	938	61340	0	4	-25	12	14370	1190	3550
370	884	59700	0	14	-10	12	14280	1210	3560
369	879	58060	0	6	-12	23	14210	1220	3580
368	860	56440	0	14	-31	14	14040	1230	3590
367	894	54960	0	12	-14	15	13820	1190	3610
366	945	53550	0	17	10	28	13590	1190	3660
365	963	51940	0	20	-4	23	13360	1160	3740
364	902	50290	0	18	-6	13	13250	1180	3740
363	880	48820	0	15	-5	15	13030	1220	3740
362	900	47390	0	4	-45	9	12860	1260	3740
361	886	45890	0	5	-30	7	12730	1360	3780
360	956	44650	0	12	8	12	12520	1440	3810
359	1000	43380	0	20	6	21	12280	1540	3910
358	947	41980	0	18	2	24	12080	1690	3950
357	973	40750	0	17	-1	27	11850	1800	3970
356	956	39410	0	12	9	22	11560	1940	3990
355	933	38220	0	4	-15	9	11290	2130	4050
354	942	37110	0	2	-12	11	11000	2320	4070
353	1010	35900	0	9	27	21	10720	2570	4160
352	989	34850	0	2	16	18	10440	2840	4220
351	967	33890	0	8	24	18	10230	3150	4330
350	987	32760	0	9	22	20	9940	3480	4400
349	964	31600	0	8	32	25	9690	3830	4470
348	968	30680	0	21	36	30	9440	4210	4580
347	995	29810	0	14	16	29	9090	4580	4650
346	984	28860	0	13	34	24	8870	4970	4700

345	930	27950	0	14	14	20	8450	5340	4750
344	1010	27130	0	21	-2	34	8080	5680	4840
343	1030	26340	0	14	-3	37	7830	6040	4900
342	1020	25550	0	16	-16	37	7560	6430	4970
341	1010	24770	0	17	-22	40	7350	6780	4980
340	988	24030	0	24	-6	34	7190	7150	5080
339	1060	23600	0	15	-30	21	6940	7450	5080
338	1030	22890	0	13	22	46	6650	7650	5160
337	1100	22350	0	10	45	37	6610	7840	5200
336	1020	21750	0	19	30	40	6400	7900	5310
335	980	21230	0	26	25	51	6290	7920	5380
334	965	20630	0	22	31	53	6150	7880	5390
333	963	20080	0	16	44	57	5900	7750	5400
332	1050	19670	0	15	43	65	5830	7600	5390
331	1090	19380	0	10	66	71	5680	7340	5390
330	954	18920	0	15	83	99	5790	7240	5420
329	1010	18450	0	26	106	118	5630	6890	5440
328	1010	18280	0	37	120	151	5460	6500	5510
327	1010	18100	0	41	147	187	5330	6230	5550
326	1050	17800	0	39	179	207	5240	5950	5490
325	1020	17490	0	26	188	232	5240	5750	5470
324	1030	17180	0	19	217	290	5230	5590	5590
323	1030	16880	0	20	279	354	5140	5400	5610
322	1020	16840	0	31	336	420	5030	5220	5640
321	1030	16570	0	39	358	487	4960	5060	5680
320	1030	16490	0	36	410	562	4870	4910	5770
319	1060	16390	0	40	438	626	4830	4760	5790
318	1130	16300	0	35	510	715	4870	4630	5800
317	1080	16180	0	35	572	795	4800	4470	5910
316	1150	16110	0	39	594	859	4740	4330	5950
315	1180	16060	0	56	622	933	4680	4210	5980
314	1120	16080	0	56	670	1010	4650	4130	6010
313	1150	16050	0	67	732	1070	4710	4100	6100
312	1190	16000	0	89	807	1140	4750	4080	6150
311	1350	16320	0	132	893	1240	4740	4090	6230
310	1450	16450	0	179	1020	1370	4680	4090	6310
309	1670	16710	1	269	1170	1510	4670	4120	6390
308	1910	16810	1	409	1360	1700	4720	4210	6540
307	2200	17060	1	616	1600	1920	4860	4390	6620
306	2750	17470	1	873	1920	2200	4930	4620	6760
305	3420	17970	1	1210	2180	2510	4980	4930	6810
304	4240	18260	1	1600	2420	2850	4990	5280	6950
303	5260	18590	1	1970	2670	3210	4990	5670	7090
302	6520	18890	1	2260	2940	3570	5050	6140	7240
301	8000	19340	1	2460	3100	3910	5060	6610	7390
300	9720	19800	1	2620	3270	4220	5080	7170	7480
299	11750	20420	1	2720	3460	4510	5090	7740	7680
298	14020	20910	1	2800	3640	4790	5080	8350	7880
297	16700	21400	1	2860	3800	5040	5120	8960	8020
296	20050	22180	1	2930	3930	5300	5260	9550	8210
295	24010	22840	2	2980	4080	5540	5340	10070	8320
294	28660	23680	2	3050	4240	5760	5490	10550	8480
293	33750	24800	2	3120	4430	6020	5720	10930	8670
292	38270	26040	2	3190	4590	6280	5900	11250	8880
291	41410	27420	2	3230	4730	6550	6320	11500	9040
290	43000	28750	2	3240	4930	6840	6660	11590	9240
289	43960	29990	2	3260	5170	7080	7130	11690	9410
288	45470	30960	3	3290	5420	7280	7700	11680	9560
287	47680	31650	3	3350	5710	7370	8370	11610	9710
286	50090	32280	3	3440	5920	7320	9270	11540	9890
285	52290	32950	3	3580	6080	7170	10310	11440	10050
284	53840	33580	3	3760	6080	6930	11520	11350	10130
283	54920	34200	4	3980	6020	6650	12750	11270	10250
282	55670	34820	4	4200	5960	6350	14120	11220	10350
281	56100	35180	4	4420	5870	6090	15340	11140	10450
280	56020	35380	4	4610	5760	5840	16540	11110	10600
279	55310	35520	5	4810	5650	5610	17650	11100	10690
278	54370	35670	5	5040	5590	5400	18360	11090	10790
277	53520	35760	5	5300	5590	5210	18840	11140	10880
276	52810	35650	6	5620	5630	5040	19020	11210	10940
275	52160	35550	6	6010	5670	4900	19010	11360	11080
274	51370	35550	6	6450	5730	4770	19000	11600	11170

273	50150	35440	7	6900	5790	4680	19030	11950	11300
272	48790	35480	7	7360	5880	4640	19070	12330	11430
271	47460	35830	8	7810	6040	4640	19200	12760	11630
270	46090	36110	8	8260	6180	4670	19340	13230	11780
269	44570	36330	9	8720	6350	4730	19470	13700	11930
268	42890	36170	9	9200	6530	4810	19630	14190	12120
267	41190	35920	10	9660	6710	4910	19640	14630	12260
266	39580	35880	10	10110	6890	5030	19620	15040	12440
265	37910	36110	11	10510	7050	5150	19420	15310	12620
264	36050	36010	12	10850	7240	5260	19120	15540	12790
263	34230	35780	12	11130	7410	5380	18830	15680	13060
262	32690	35870	13	11330	7500	5500	18440	15780	13360
261	31210	36040	14	11440	7610	5620	18190	15990	13610
260	29850	36080	15	11470	7690	5770	17910	16240	13880
259	28490	36200	16	11430	7780	5910	17630	16660	14180
258	26980	36100	17	11330	7870	6070	17400	17240	14510
257	25460	35790	18	11190	7940	6260	17180	17970	14890
256	24200	35740	19	11010	8060	6480	16970	18880	15390
255	23270	35930	20	10770	8140	6710	16910	20060	15810
254	22560	36310	21	10520	8270	6990	16910	21530	16320
253	22010	36640	22	10230	8400	7310	16980	23350	16890
252	21580	37010	23	9910	8590	7680	17360	25700	17490
251	21310	37390	24	9600	8810	8100	17810	28520	18180
250	21500	38220	26	9300	9050	8610	18630	31930	18910
249	22170	39470	27	9020	9340	9180	19720	35880	19650
248	23250	40940	29	8760	9720	9810	20830	40120	20440
247	24660	42610	30	8550	10120	10490	22360	44320	21220
246	26710	44900	32	8420	10620	11260	24130	48060	21960
245	29610	47700	34	8350	11200	12100	26370	50890	22680
244	33460	51290	35	8370	11840	13010	29250	52510	23290
243	38550	55920	37	8490	12540	14030	32110	52920	23860
242	45110	61450	39	8740	13390	15170	34850	52240	24360
241	53450	67980	41	9120	14440	16400	37060	50840	24770
240	63850	75670	44	9630	15560	17690	38830	48960	25080
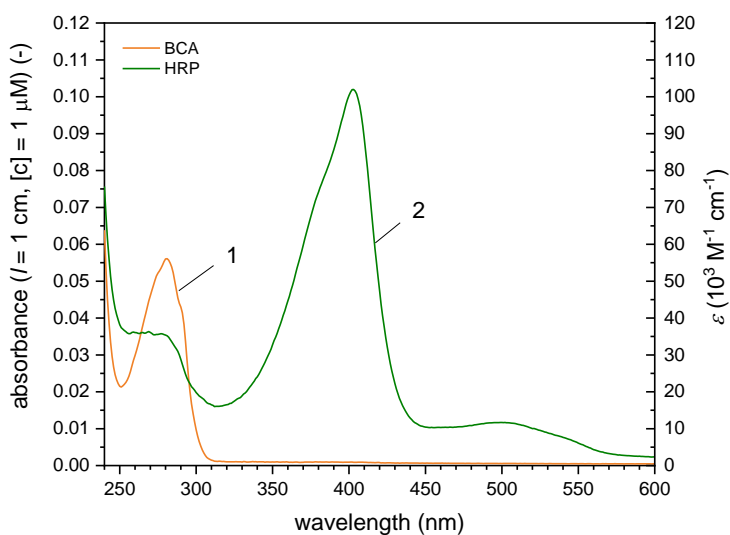
Figure S-6. UV/vis absorption spectra of BCA (1, orange) and HRP (2, green). The measured spectra were adjusted to ε_{280} (BCA) = 5.6·10^4 M^{-1}cm^{-1} and ε_{403} (HRP) = 1.02·10^5 M^{-1}cm^{-1}, respectively (see section 2.1.).

8. Oxidation of DCF in the presence of HRP and H$_2$O$_2$
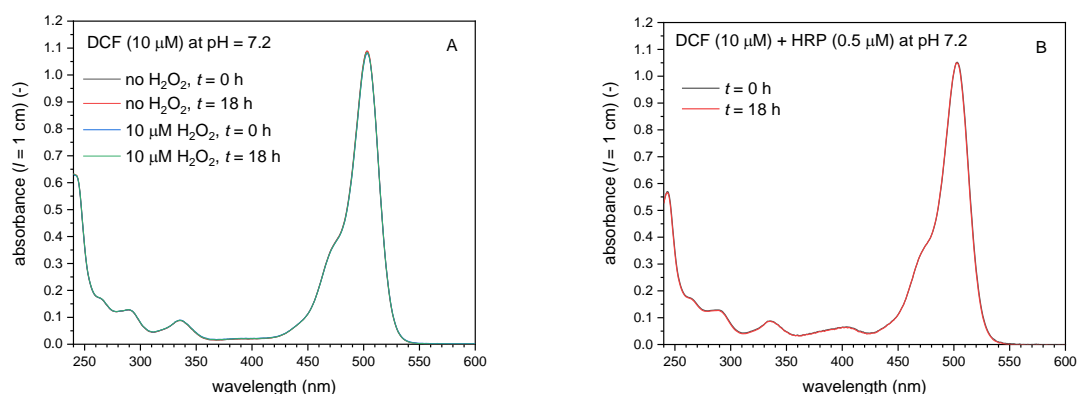
Figure S-7. Stability of DCF (10 μM) in PB (10 mM sodium phosphate buffer solution, pH = 7.2) at T = 25 °C, **(A)** *without added H$_2$O$_2$ or HRP* (18 h), *in the presence of H$_2$O$_2$* (9 μM, 72 h) without HRP; and **(B)** *in the presence of HRP* (0.5 μM, 18 h) without H$_2$O$_2$. For each stability test, the absorption spectrum was measured every 5 min against PB by keeping the solutions in the spectrophotometer (path length l = 1 cm). Under the condition used, DCF was stable as no significant change in the absorption spectrum could be detected.
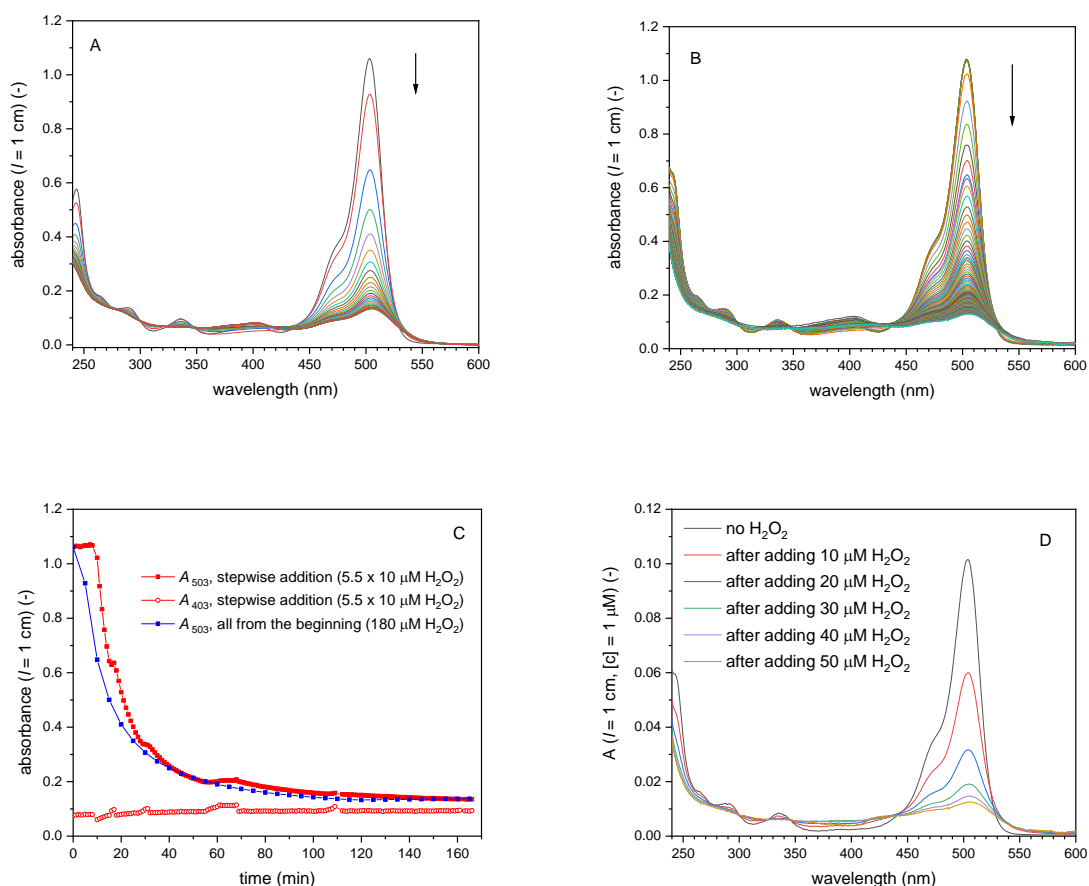
Figure S-8. Oxidation of DCF in PB (10 mM sodium phosphate buffer solution, pH = 7.2) at T = 25 °C with HRP and H_2O_2.

(A) $[DCF]_0$ = 10 µM, [HRP] = 0.5 µM, $[H_2O_2]_0$ = 180 µM *added at once*. The spectrum was recorded every 5 min for 180 min. A_{503} decreased with time. Addition of more H_2O_2 did not lead to a further decrease in A_{503}.

(B) $[DCF]_0$ = 10 µM, [HRP] = 0.5 µM, with *stepwise addition* of H_2O_2 (10 µM) up to 55 µM. The spectrum was recorded every 10 min. After each H_2O_2 addition, the spectrum was recorded until it did not change anymore. Then the next portion of H_2O_2 was added, up to a total of 5.5 equivalents with respect to $[DCF]_0$. After addition of 5 equivalents H_2O_2 (50 µM), the spectrum did not change anymore.

(C) Comparison of the two DCF oxidation experiments shown in **(A)** and **(B)**. Changes in A_{503} and A_{403}. The data for A_{403} reflect transient changes in the oxidation state of the heme group in HRP.[S9, S10]

(D) Stable absorption spectra after stepwise addition of H_2O_2, from top to bottom: DCF only (10 µM, no H_2O_2), after addition of 10, 20, 30, 40, 50 or 55 µM H_2O_2 (and waiting until equilibrium was reached). From the recorded spectra, the spectrum of HRP (0.5 µM, see **Figure S-6**) was subtracted and they were normalized to 1 µM with respect to the concentration and volume of the initial DCF solution. The last two spectra were identical and taken as the spectrum of DCF_{ox}. Oxidation of DCF is indicated by the increase in absorbance at λ = 530-550 nm, see Rota et al. (1999).[S11]

9. Catalase-like activity of HRP under similar conditions as used for reactions with DCF derivatives in bulk solution
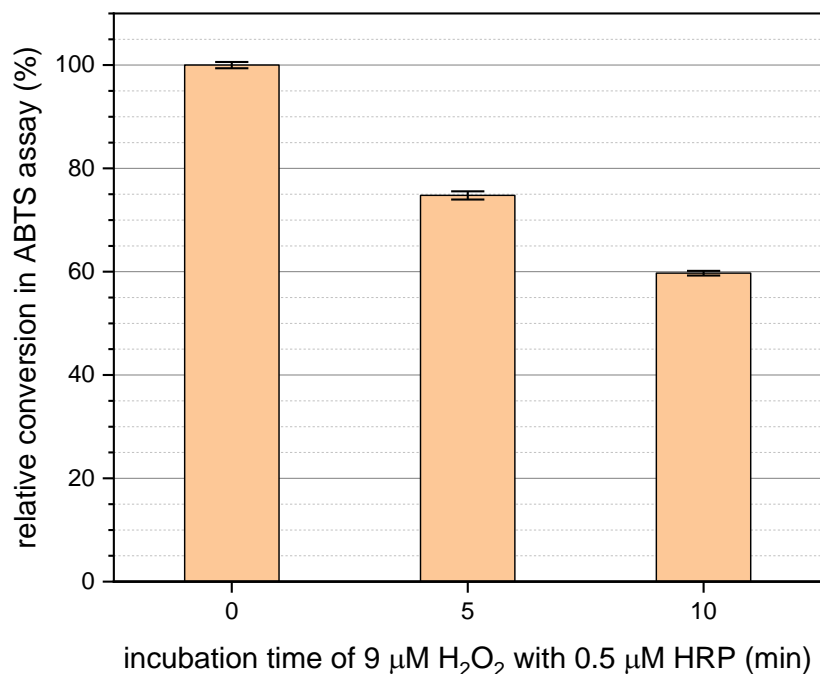
Figure S-9. Decreasing H_2O_2 concentrations observed with the ABTS assay. HRP (0.5 μM) and H_2O_2 (9 μM) were mixed in PB (10 mM phosphate buffer solution, pH 7.2). Either at the same time or after 5 or 10 min incubation time in light-shielded polypropylene tubes, $ABTS^{2-}$ (1 mM) was added to the solutions that were placed in a 1 cm quartz cell. After mixing by pipette, UV/vis spectra were recorded until A_{414} became stable (A_{414} indicated formation of $ABTS^{•-}$, the reaction was finished within the first 10 seconds). After subtracting A_{414} contributions from HRP and the $ABTS^{2-}$ substrate solution in PB, the obtained ΔA_{414} was attributed relatively to the amount of H_2O_2 present at the time of $ABTS^{2-}$ addition (that was converted to $ABTS^{•-}$ proportionally). It was clearly shown that under the conditions used (HRP 0.5 μM in PB), the concentration of H_2O_2 significantly decreased over time. This can be attributed to the HRP-catalysed decomposition of H_2O_2 ("catalaytic" activity of HRP).[S12]

10. Hydrolysis of DCFH₂-DA catalysed by BCA

Control measurements 1
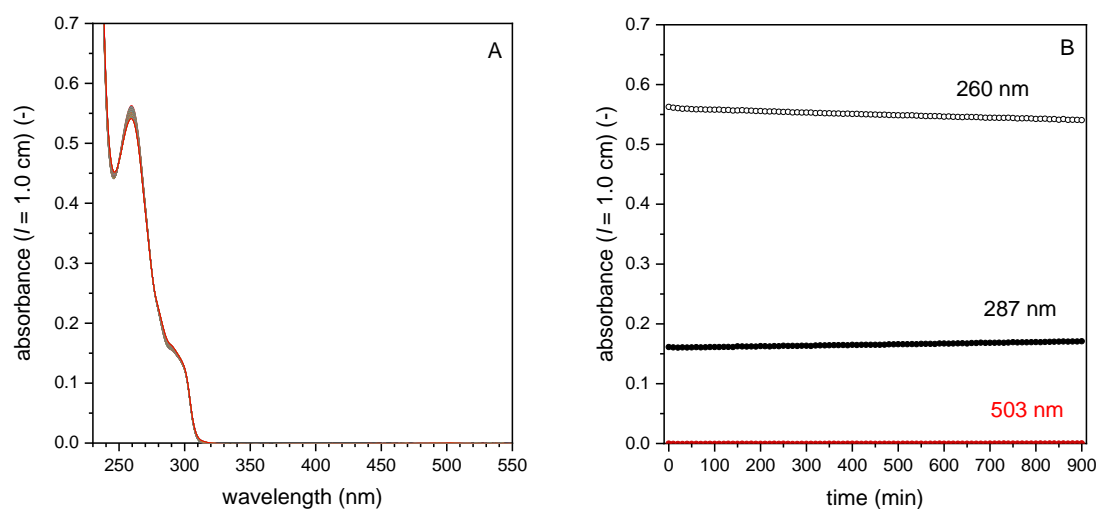
Figure S-10. Stability of DCFH$_2$-DA (50 µM, 1 vol% DMSO) in PB (10 mM sodium phosphate buffer solution, pH = 7.2) at 25 °C, determined by recording the UV/vis spectrum as a function of time. **(A)** Change in the spectrum, as recorded every 10 min for 15 h. **(B)** Changes of A_{260}, A_{287}, and A_{503}.
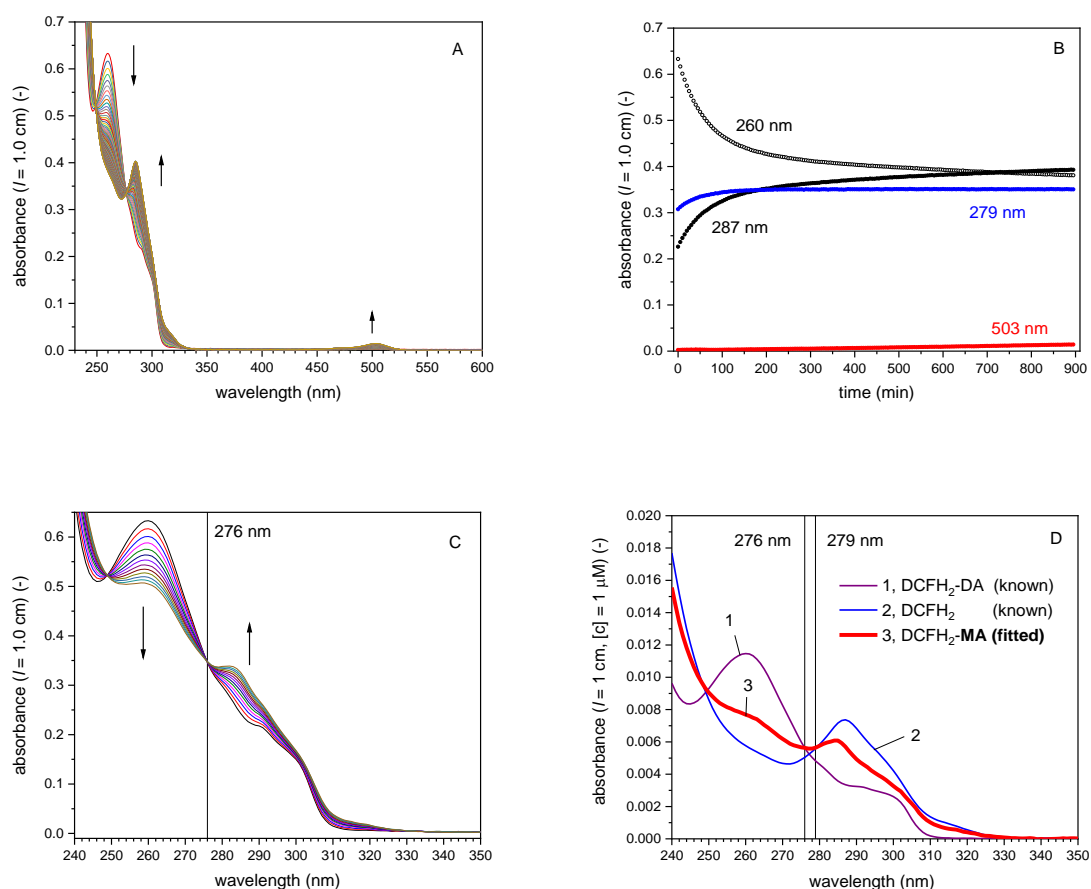
Control measurements 2
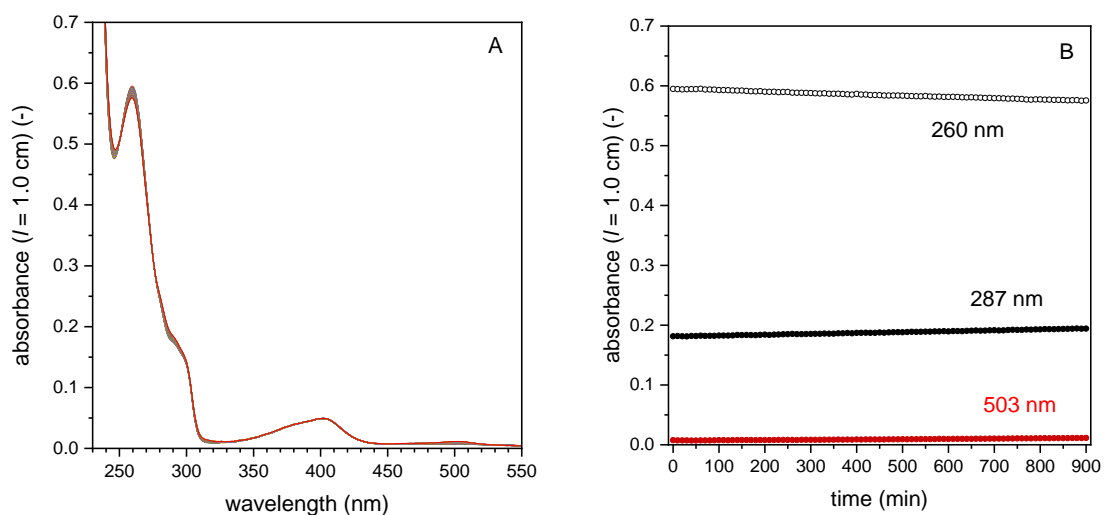
Figure S-11. Stability of DCFH$_2$-DA (50 µM, 1 vol% DMSO) in PB (10 mM sodium phosphate buffer solution, pH = 7.2) at 25 °C in the presence of HRP (0.5 µM). **(A)** Change in the UV/vis absorption spectrum, recorded every 10 min for 15 h. **(B)** Changes of A_{260}, A_{287}, and A_{503}. The absorption band with maximal absorption at 403 nm originated from the heme group of HRP.[S8, S13]

Control measurements 3
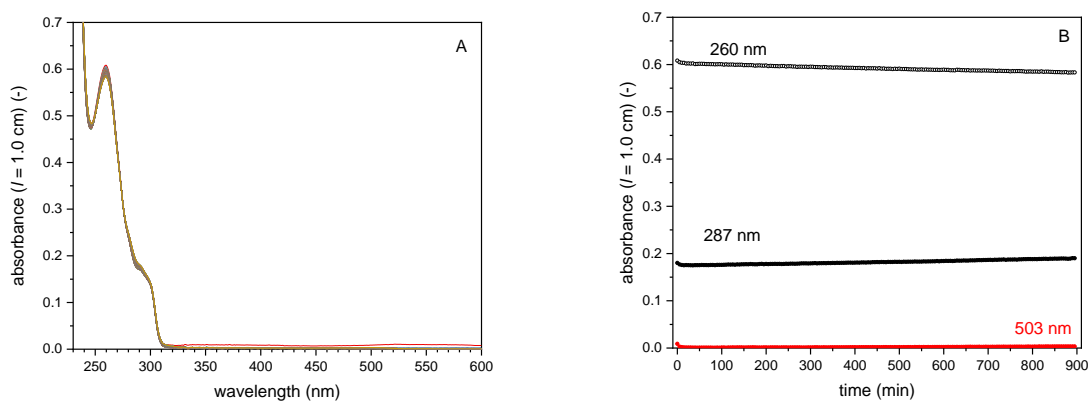
Figure S-12. Stability of DCFH$_2$-DA (50 µM, 1 vol% DMSO) in PB (10 mM sodium phosphate buffer solution, pH = 7.2) at 25 °C in the presence of H$_2$O$_2$ (9 µM). **(A)** Change in the UV/vis absorption spectrum, recorded every 5 min for 15 h. **(B)** Changes of A_{260}, A_{287}, and A_{503}.
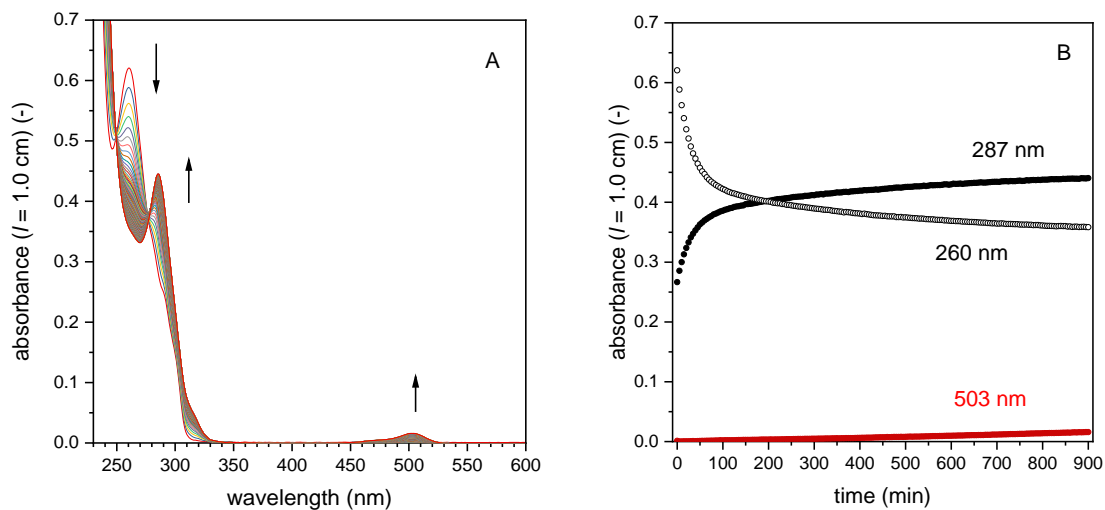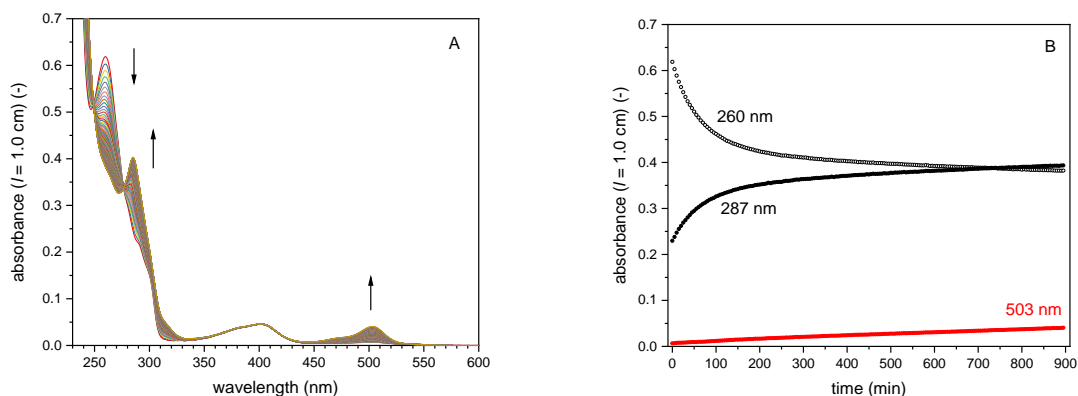
Figure S-13. BCA-catalysed hydrolysis of DCFH$_2$-DA (50 µM, 1 vol% DMSO) in PB (10 mM sodium phosphate buffer solution, pH = 7.2) at 25 °C. [BCA] = 1.0 µM. **(A)** Change in the UV/vis absorption spectrum, recorded every 5 min for 15 h. **(B)** Changes of A_{260}, A_{287}, A_{279} and A_{503}. After t = 900 min, A_{503} was 0.014, corresponding to 0.14 µM DCF (ε_{503} (DCF) = 1.02·10^5 M^{-1}cm^{-1}, see **Figure S-3**). At λ = 279 nm, the isosbestic point between DCFH$_2$ and DCFH$_2$-MA becomes visible with stable absorption the latest after t = 300 min (no DCFH$_2$-DA left). **(C)** Change in the UV/vis absorption spectrum, recorded every 5 min within the first 60 min of reaction. At λ = 276 nm, the isosbestic point between DCFH$_2$-DA and DCFH$_2$-MA becomes visible, as the small early DCFH$_2$ formation can be neglected. **(D)** Absorption spectra of DCFH$_2$-DA (1), DCFH$_2$ (2) (both known, see **Figure 2**) and DCFH$_2$-MA (3) (fitted). With help of the two isosbestic points of DCFH$_2$-MA (at 276 nm with DCFH$_2$-DA and at 279 nm with DCFH$_2$), the molar absorption spectrum could be fitted from the time evolution of the reaction between t = 300-900 min (see **B**). Thereby, DCFH$_2$-MA hydrolysis was assigned to the differential spectrum (A$_{900min}$ – A$_{300min}$) in such a concentration that the resulting molar fit for DCFH$_2$-MA (adding the molar differential spectrum to the known spectrum of DCFH$_2$) complied with both isosbestic points (both isosbestic points are from different reaction phases and thereby independent).
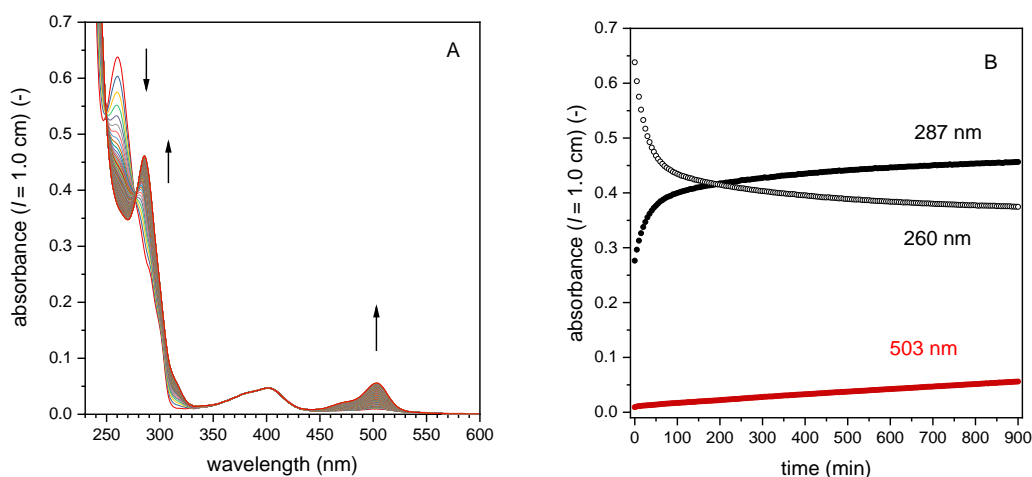
Figure S-14. BCA-catalysed hydrolysis of DCFH$_2$-DA (50 µM, 1 vol% DMSO) in PB (10 mM sodium phosphate buffer solution, pH = 7.2) at 25 °C. [BCA] = 2.0 µM. **(A)** Change in the UV/vis absorption spectrum, recorded every 5 min for 15 h. (B): Changes of A_{260}, A_{287}, and A_{503}. After t = 900 min, A_{503} was 0.016, corresponding to 0.16 µM DCF (ε_{503} (DCF) = 1.02·10^5 M^{-1}cm^{-1}, see **Figure S-3**).
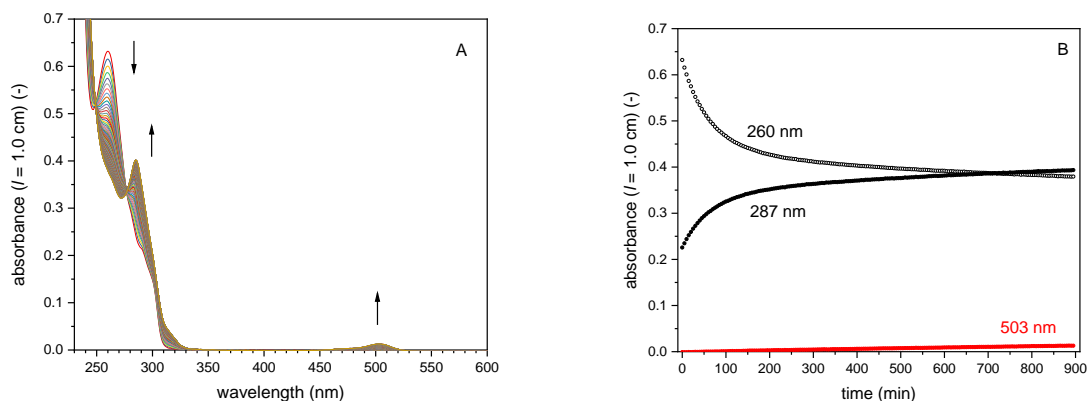
Figure S-15. BCA-catalysed hydrolysis of DCFH$_2$-DA (50 µM, 1 vol% DMSO) in PB (10 mM sodium phosphate buffer solution, pH = 7.2) at 25 °C in the presence of HRP (0.5 µM). [BCA] = 1.0 µM, *no* added H$_2$O$_2$. **(A)** Change in the UV/vis absorption spectrum, recorded every 5 min for 15 h. **(B)** Changes of A$_{260}$, A$_{287}$, and A$_{503}$. After *t* = 900 min, A$_{503}$ was 0.04, corresponding to 0.4 µM DCF (ε_{503} (DCF) = 1.02·10^5 M^{-1}cm^{-1}, see **Figure S-3**).

Figure S-16. BCA-catalysed hydrolysis of DCFH$_2$-DA (50 µM, 1 vol% DMSO) in PB (10 mM sodium phosphate buffer solution, pH = 7.2) at 25 °C in the presence of HRP (0.5 µM). [BCA] = 2.0 µM, *no* added H$_2$O$_2$. **(A)** Change in the UV/vis absorption spectrum, recorded every 5 min for 15 h. **(B)** Changes of *A*$_{260}$, *A*$_{287}$, and *A*$_{503}$. After *t* = 900 min, *A*$_{503}$ was 0.056, corresponding to 0.55 µM DCF (ε_{503} (DCF) = 1.02·10^5 M^{-1}cm^{-1}, see **Figure S-3**).

Control measurements 6

Figure S-17. BCA-catalysed hydrolysis of DCFH$_2$-DA (50 μM, 1 vol% DMSO) in PB (10 mM sodium phosphate buffer solution, pH = 7.2) at 25 °C in the presence of H$_2$O$_2$ (9 μM) *without* HRP. [BCA] = 1.0 μM. **(A)** Change in the UV/vis absorption spectrum, recorded every 5 min for 15 h. **(B)** Changes of A_{260}, A_{287}, and A_{503}. After t = 900 min, A_{503} was 0.013, corresponding to 0.13 μM DCF (ε_{503} (DCF) = 1.02·10^5 M^{-1}cm^{-1}, see **Figure S-3**).

Control measurements 7
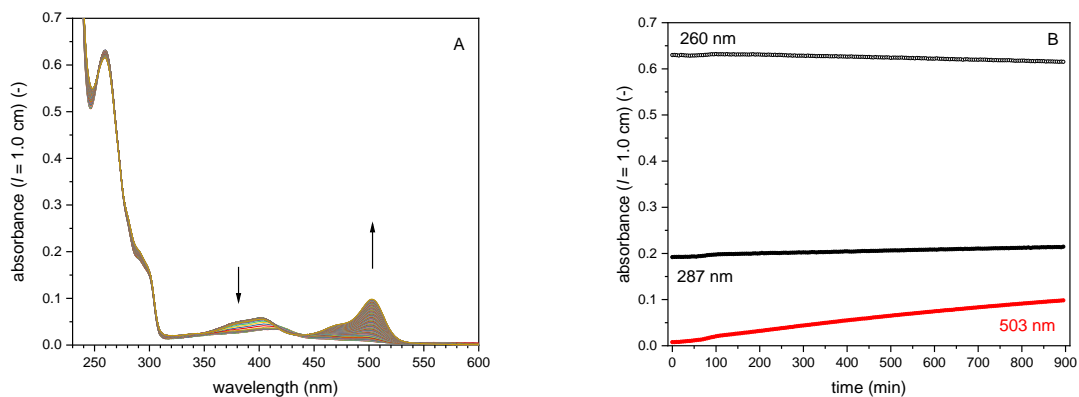
Figure S-18. Non-enzymatic hydrolysis of DCFH$_2$-DA (50 μM, 1 vol% DMS) in PB (10 mM sodium phosphate buffer solution, pH = 7.2) at 25 °C in the presence of HRP (0.5 μM) and H$_2$O$_2$ (9 μM) *without* BCA. **(A)** Change in the UV/vis absorption spectrum, recorded every 5 min for 15 h. **(B)** Changes of A_{260}, A_{287}, and A_{503}. After t = 900 min, A_{503} was 0.1, corresponding to 0.98 μM DCF (ε_{503} (DCF) = 1.02·10^5 M^{-1}cm^{-1}, see **Figure S-3**).

11. Specificity constants (k_{cat}/K_M) for the BCA-catalysed hydrolysis of DCFH₂-DA, DCFH₂-MA and DCF-MA in bulk solution

Table S-2. Specificity constants (or kinetic efficiencies), k_{cat}/K_M (Michaelis-Menten kinetics), for the hydrolysis of DCFH₂-DA, DCFH₂-MA and DCF-MA catalysed by BCA. The experimentally measured initial rates of hydrolysis were linearly dependent on the concentration of BCA used ($[E]_0$) and on the current substrate concentration ($[S]$). Due to this linear dependency and BCA being rather inefficient in catalysing the hydrolysis of these substrates, Michaelis-Menten kinetics for $[S] \ll K_M$ was assumed to apply. Under these conditions, the reaction rate is linearly dependent on $[S]$ and $[E]_0$ and the rate constant is k_{cat}/K_M, such that: $d[S]/dt = (k_{cat}/K_M) \cdot [E]_0 \cdot [S]$. Thus, first order kinetics applies, such that $[S]_t = [S]_0 \cdot e^{-kt}$, whereas $k = (k_{cat}/K_M) \cdot [E]_0$. The experimentally determined decrease of $[S]_t$ with time was fitted as exponential decay with time and the obtained value for k was divided by $[E]_0$ to get k_{cat}/K_M. 10 mM sodium phosphate buffer solution, pH = 7.2, 25 °C.

Substrate (Reaction Step in **Scheme 2**)	k_{cat}/K_M (μM^{-1} min^{-1})	Initial experimental conditions	Fitting conditions (Respective figure with data)
DCFH₂-DA[a] (Hyd_1)	**0.0187**	50 µM DCFH₂-DA 1.0 µM BCA	t = 0-300 min, R^2=0.99891 (**Figure 3A**, purple data points)
	0.0209	50 µM DCFH₂-DA 2.0 µM BCA	t = 0-200 min, R^2=0.99912 (**Figure 3B**, purple data points)
DCFH₂-MA[b] (Hyd_2)	**0.0012**	50 µM DCFH₂-DA 2.0 µM BCA	t = 200-900 min, R^2=0.99948 (**Figure 3B**, red data points)
DCF-MA[b] (Hyd_3)	**0.0043**	20 µM DCF-DA 1.0 µM BCA	t = 200-500 min, R^2=0.99928 (**Figure S-19C**, red data points)
DCF-MA within cascade reaction, thus coexisting DCFH₂-DA and DCFH₂-MA[c] (Hyd_3)	**0.0050**	50 µM DCFH₂-DA 2.0 µM BCA 0.5 µM HRP 9 µM H₂O₂	t = 50-350 min, R^2=0.99992 (DCF-MA concentration calculated from A_{503} and A_{460} in **Figure 5**, blue data points)
	0.0048	50 µM DCFH₂-DA 3.0 µM BCA 0.5 µM HRP 9 µM H₂O₂	t = 50-350 min, R^2=0.99990 (DCF-MA concentration calculated from A_{503} and A_{460} in **Figure 5**, red data points)

[a] The increasing amount of DCFH₂-MA (resulting from the hydrolysis of DCFH₂-DA) did not have a significant impact on d[DCFH₂-DA]/dt. No product inhibition was observed, although the hydrolysis of DCFH₂-MA was also catalysed by BCA. The reason could be a low ES-complex concentration which is usual for $[S] \ll K_M$, and thus not many BCA enzyme molecules were blocked by other substrates.
[b] The DCFH₂-MA and DCF-MA concentrations were taken into account after the concentrations of DCFH₂-DA and DCF-DA, respectively, were approaching zero.
[c] The respective k_{cat}/K_M was found to be similar for different enzyme concentrations within the cascade reaction as well as for an "undisturbed" DCF-MA/DCF mixture (entry above), including higher DCF-species concentration (50 µM as opposed to 20 µM). Although [DCF-MA] within the time frame used for the fitting was smaller than coexisting [DCFH₂-DA] + [DCFH₂-MA], no significant impact on d[DCF-MA]/dt was found within the cascade reaction. No competitive inhibition by the reduced DCF-species was observed, although the hydrolysis of DCFH₂-DA and DCFH₂-MA was also catalysed by BCA at the same time. The reason could be a low ES-Complex concentration, which is usual for $[S] \ll K_M$, and thus not many BCA enzymes being blocked by other substrates.

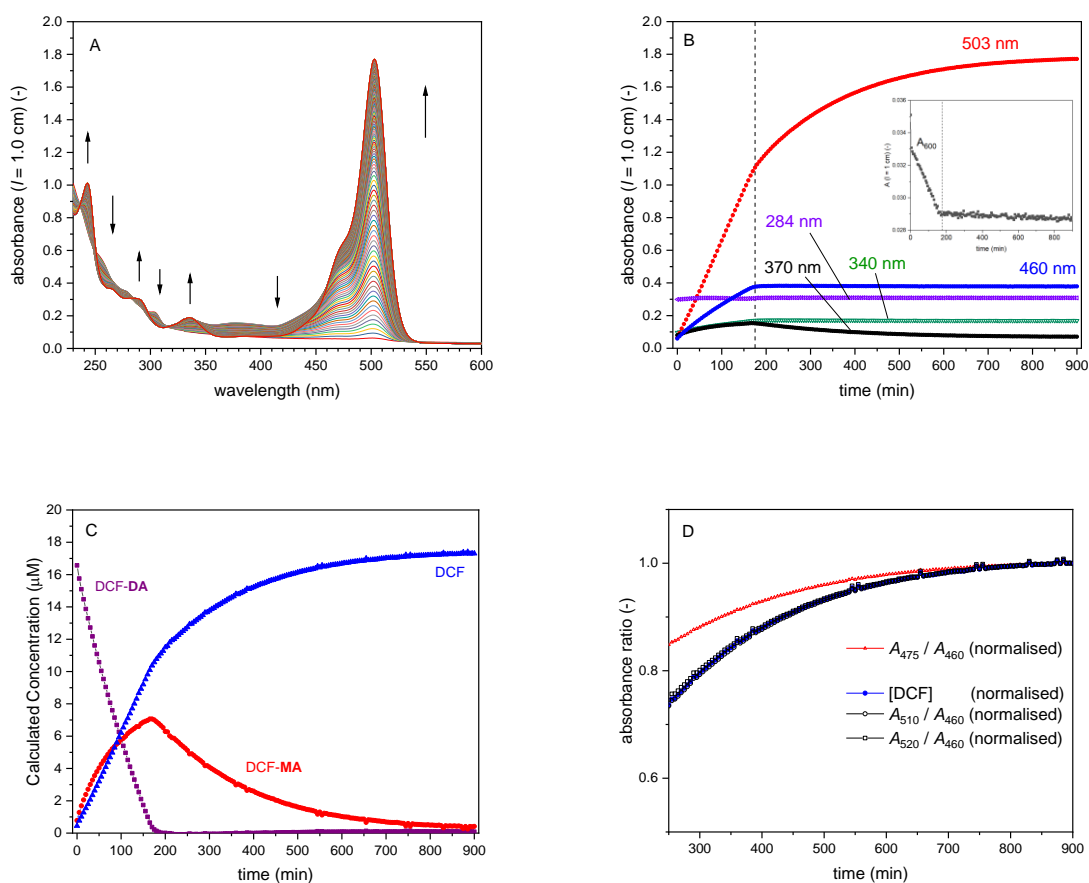## 12. Hydrolysis of DCF-DA catalysed by BCA

Figure S-19. BCA-catalysed hydrolysis of DCF-DA (20 µM, 1 vol% DMSO) in PB (10 mM sodium phosphate buffer solution, pH = 7.2) at 25 °C. [BCA] = 1.0 µM. **(A)** Change in the UV/vis absorption spectrum, recorded every 5 min for 15 h. **(B)** Changes of A_{503}, A_{460}, A_{370}, A_{340} and A_{284}. A_{503} can be mainly attributed to the formation of DCF, and A_{370} to DCF-MA. After an initial reaction phase (up to the dashed vertical line at t = 175 min), isosbestic points were at λ = 284, 340 and 460 nm. After t = 175 min, all DCF-DA molecules were at least partially hydrolysed (presence of only DCF-MA and DCF). As the samples were turbid at the beginning of the reaction (see inset), no quantitative analysis was performed during the initial phase of the reaction (initial hydrolysis of DCF-DA). **(C)** Concentration determination during the reaction, using the known absorbance of DCF at λ = 520 nm (ε_{520} (DCF) = $2.7 \cdot 10^4$ M^{-1}cm^{-1}) and the isosbestic point between DCF-MA/DCF at λ = 460 nm (ε_{460} (DCF-MA/DCF) = $1.98 \cdot 10^4$ M^{-1}cm^{-1}). **(D)** Comparison of the time course of A_{520}, A_{510} and A_{475} with the rising DCF concentration. All values were normalised to the value observed at t = 900 min. Whereas the ratio for A_{520} and A_{510} aligned well with the calculated concentration of DCF, A_{475} (as an arbitrary example at a wavelength at which DCF-MA absorbs light) did deviate. This shows that DCF-MA does not absorb at λ > 510 nm, which was used to fit the molar absorption spectrum of DCF-MA (see 3.1.3 and **Figure 2**). For the BCA-catalysed hydrolysis of DCF-MA, the specificity constant (k_{cat}/K_M) was determined (see **Table S-2**).

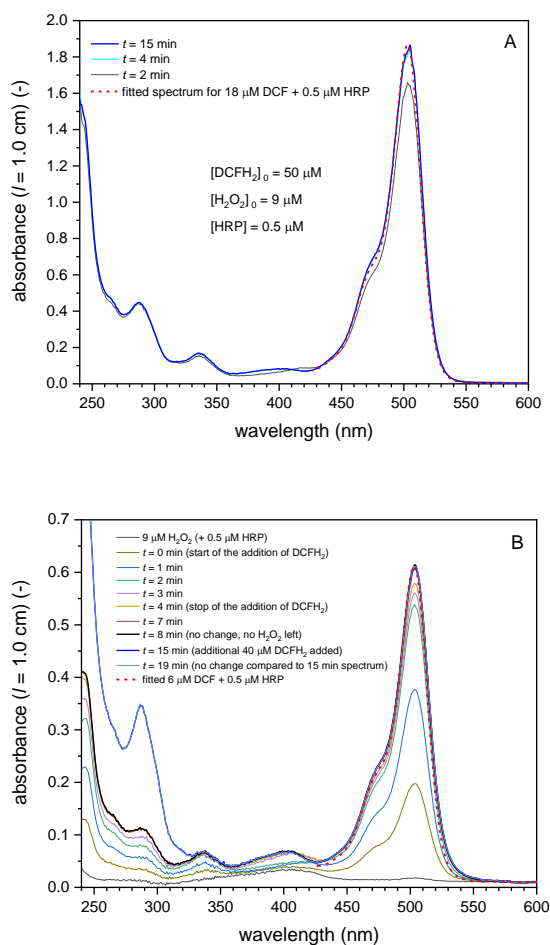## 13. Oxidation of DCFH$_2$ catalysed by HRP with H$_2$O$_2$ as oxidant

Figure S-20. HRP-catalysed oxidation of DCFH$_2$ (50 µM) in PB (10 mM sodium phosphate buffer solution, pH = 7.2) at 25 °C, [HRP] = 0.5 µM, [H$_2$O$_2$]$_0$ = 9 µM. **(A)** Solutions of DCFH$_2$, HRP, and H$_2$O$_2$ were mixed at the beginning, and the UV/vis spectrum of the reaction mixture was measured after t = 2, 4, and 15 min. The latter spectrum (blue curve) was identical with the spectrum of a 18 µM solution of DCF (red line) between λ = 430 and 600 nm, as calculated from the reference spectrum of DCF given in **Figure 2B**. As a result, the two-electron reduction of H$_2$O$_2$ yielded quantitative conversion of DCFH$_2$ to DCF according to **Scheme 1**: One-electron oxidations of two molecules of DCFH$_2$ to DCFH$^\bullet$ (Oxi_1'a and Oxi_1'b), followed by one-electron oxidations of two molecules of DCFH$^\bullet$ to two molecules of DCF with dissolved O$_2$ (Oxi_1''). **(B)** DCFH$_2$ was added in portions to the reaction mixture. 10 µM DCFH$_2$ were added slowly during the first 4 min. After the UV/vis spectrum did not change anymore with time (t = 8 min), the remaining 40 µM DCFH$_2$ were added (t = 15 min). This final addition did not lead to a further change of the absorption spectrum above λ = 330 nm. Spectral changes below λ = 330 nm were due to DCFH$_2$. This clearly indicates that H$_2$O$_2$ (9 µM initially added) reacted only with the initially added DCFH$_2$ (10 µM), resulting in the formation of DCF and DCF$_{ox}$. Moreover, another part of the added H$_2$O$_2$ was probably oxidized to O$_2$ *via* the catalatic activity of HRP (see **Figure S-9**).[S12, S14] In any case, the final spectrum could not be fitted well with the spectrum of DCF only (red dashed line), see the deviations at λ = 425 - 450 nm and at λ = 525-550 nm. They are clear indications of DCF overoxidation. In any case, the amount of DCF obtained was much lower than in the case of the experiments in **(A)**, A_{503} = 0.61 **(B)** vs A_{503} = 1.83 **(A)**.

14. Quantitative analysis of different cascade reaction mixtures run in bulk solution with dissolved enzymes

Table S-3. Summary of the quantitative analyses of various bulk cascade reaction mixtures, prepared in PB (pH = 7.2) at $[DCFH_2\text{-}DA]_0$ = 50 µM and different concentrations of BCA, HRP, and H_2O_2, kept for t = 15 h at room temperature. The concentrations given for the DCF derivatives in the final spectrum (t = 15 h) were determined by spectral fitting on the basis of isosbestic points (λ_{iso}, see **Table 1**) and characteristic absorptions (*e.g.* A_{503} for DCF or A_{550} for DCF_{ox}), using the reference spectra given in **Figure 2** and **Table S-1**. For examples, see **Figure 4C** or **Figure 13**.

Starting conditions: $[DCFH_2\text{-}DA]_0$ = 50 µM, PB: 10 mM sodium phosphate buffer solution, pH = 7.2			Determined concentrations in the reaction mixtures after a reaction time of 15 h							
[BCA] (µM)	[HRP] (µM)	$[H_2O_2]_0$ (µM)	$[DCFH_2\text{-}DA]$ (µM)	$[DCFH_2\text{-}MA]$ (µM)	$[DCFH_2]$ (µM)	[DCF-MA] (µM)	[DCF] (µM)	$[DCF_{ox}]$ (µM)	Extent of hydrolysis (%)[a]	Extent of over-oxidation (%)[b]
1	0.5	9	0	11.5	30.9	0	7.6 (42%)[c]	1.0	77	12
2	0.5	9	0	5.0	36.0	0	9.3 (52%)[c]	0.6	90	6
3	0.5	9	0	2.9	38.1	0	9.6 (52%)[c]	0.3	94	3
1	0.5	4.5	0	15.3	31.7	0	4.9 (54%)[c]	0.5	71	9
1	0.5	9	0	11.5	30.9	0	7.6 (42%)[c]	1.0	77	12
1	0.5	18	0	9.0	27.3	0	12.4 (34%)[c]	2.0	82	14
1	0.5	27	0	7.0	24.0	0	15.7 (29%)[c]	3.5	86	18
1	0.5	180	0	n/a [d]	n/a [d]	n/a [d]	24.0 [d] (7%)[c]	26.0 [d]	n/a [d]	52[d]
1	0.0050	9	0	18.2	17.3	0.4	14.2 (80%)[c]	0	63	0
1	0.0075	9	0	18.9	16.8	0.4	14.4 (80%)[c]	0	62	0
1	0.5	9	0	11.5	30.9	0	7.6 (42%)[c]	1.0	77	12
1	1	9	0	9.7	33.3	0	7.1 (39%)[c]	1.1	81	13
1	1.5	9	0	10.4	33.6	0	6.7 (37%)[c]	1.1	80	14
1	0	0	0	24.6	28.0	n/a	n/a	n/a	53	n/a
2	0	0	0	6.2	43.8	n/a	n/a	n/a	88	n/a

n/a: not applicable

Colour code: yellow, data to **Figure 5**; blue, data to **Figure 6**; red, data to **Figure 7**, green, data to **Figure 3**

[a] The extent of hydrolysis was determined by subtracting the total concentration of the remaining mono-acetate species ($[DCFH_2\text{-}MA]_{15\,h}$ + $[DCF\text{-}MA]_{15h}$) from $[DCFH_2\text{-}DA]_0$.
[b] Defined as ($[DCF_{ox}]_{15\,h}$ / ($[DCF_{ox}]_{15\,h}$ + $[DCF]_{15\,h}$))· 100 (%).
[c] Yield compared to a maximal theoretic conversion/consumption of 1 H_2O_2 for yielding 2 DCF.
[d] The complete final spectrum of the reaction mixture initially containing a large excess of H_2O_2 could not be fitted convincingly. However, from the spectral region between λ = 460 and 600 nm, the ratio between DCF and DCF_{ox} was estimated.

31

15. Kinetic reaction pathway analysis for the cascade reaction run in bulk solution depending on the HRP concentration
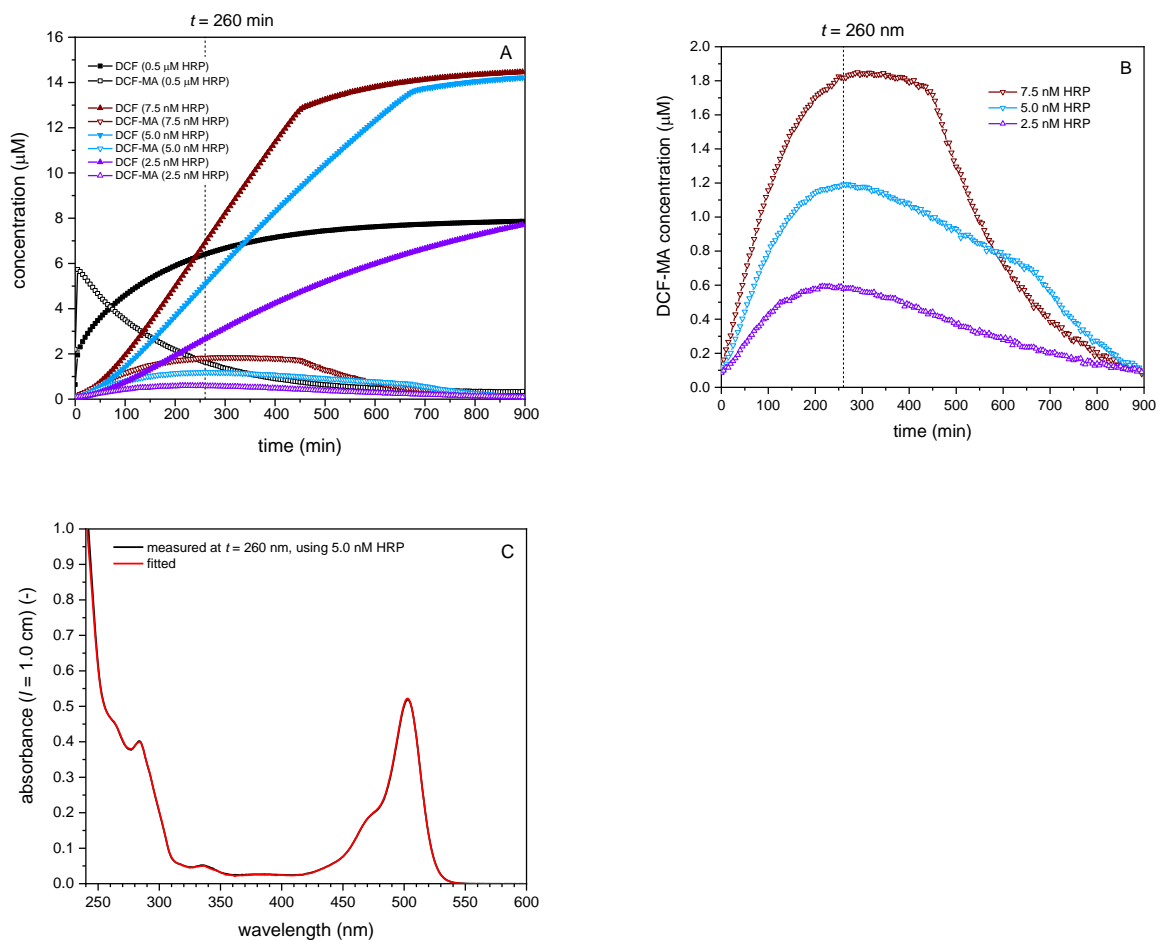

Figure S-21. (A) Concentration of DCF and DCF-MA against time in cascade reactions using 50 µM DCFH$_2$-DA, 9 µM H$_2$O$_2$, 1.0 µM BCA as well as 0.5 µM or 7.5 nM, 5.0 nM or 2.5 nM HRP (in 10 mM phosphate buffer solution, pH = 7.2, at 25 °C). The concentrations were calculated from A_{503} and A_{460}, as shown in **Figure 7**. **(B)** DCF-MA concentration for those reactions in (A) which were run with 7.5 nM, 5.0 nM, or 2.5 nM HRP. **(C)** Comparison of the spectrum measured after t = 260 min for the reaction shown in (A) using 5.0 nM HRP (black line) with the sum of the spectra obtained by fitting (red line). The concentrations of the individual species present in the reaction mixture after t = 260 min were determined by spectral fitting, as described in the caption of **Table S-3** (except for t = 260 min instead of 15 h). The following concentrations resulted from fitting: [BCA] = 1.0 µM; [HRP] = 5.0 nM; [DCFH$_2$-DA] = 0 µM; [DCFH$_2$-MA] = 40.1 µM; [DCFH$_2$] = 4.5 µM; [DCF-MA] = 1.2 µM; [DCF] = 5.0 µM; [DCF$_{ox}$] = 0 µM.

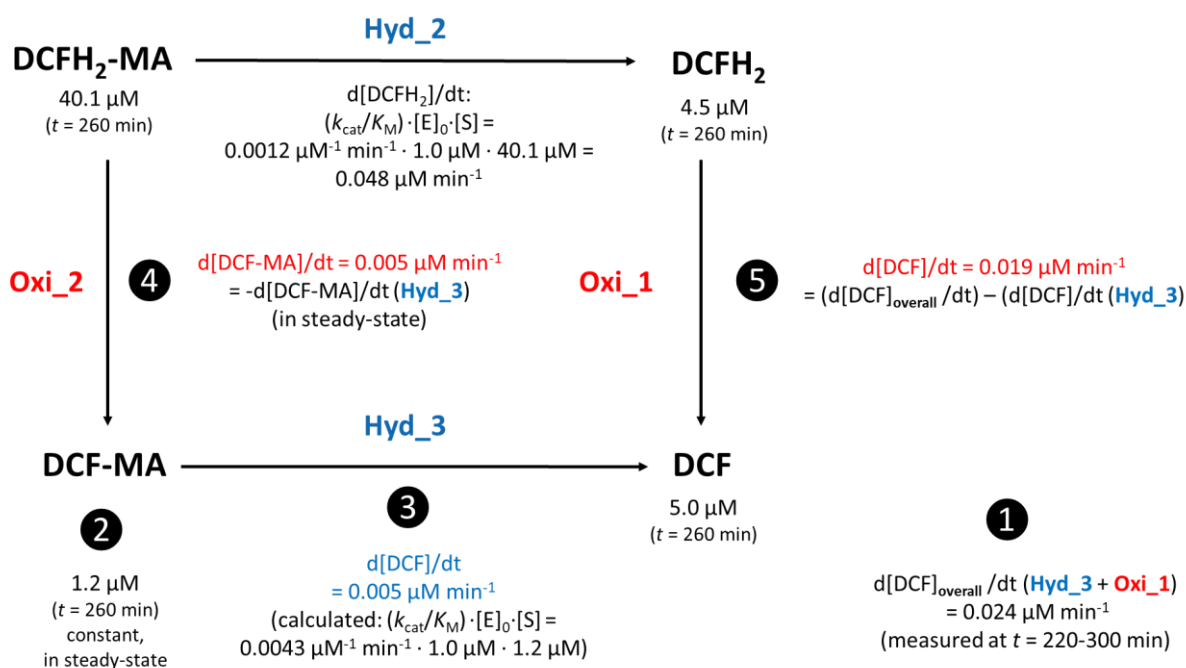Reaction pathway analysis for a **"hydrolysis-limited"** reaction ([HRP] = 0.5 µM in **Figure S-21A**):

Most of the oxidation reactions were completed after t = 5 min where H_2O_2 was nearly used up (**Figure S-21A)**. At that time, most of the oxidised species was still DCF-MA (1 µM DCF_{ox} neglected). This indicates that the reaction proceeded predominantely along *pathway 2* (see **Scheme 2**). The concentration change after 5 min was solely caused by the hydrolysis of DCF-MA to DCF (also part of *pathway 2*). Since the hydrolysis reactions were rate limiting for DCF+DCF-MA formation, a substantial part of H_2O_2 was finally not used for DCF formation. This could be attributed to some overoxidised DCF found (DCF_{ox}) and "catalatic" activity of "excess" HRP (see section 3.1.4 and **Figure S-9**).

Reaction pathway analysis for **"oxidation-limited"** reactions ([HRP] = 2.5, 5.0 and 7.5 nM in **Figure S-21A**):

The oxidation reactions took much longer (H_2O_2 was used up at t = 450 min for 7.5 nM HRP, t = 650 min for 5.0 nM HRP and not yet within the used experiment time for 2.5 nM HRP, **Figure S-21A**). The formation of DCF-MA (*via* oxidation of $DCFH_2$-MA) and its hydrolysis occurred in parallel as long as H_2O_2 was still present (see **Scheme 2**). At the beginning of the reaction, similar DCF and DCF-MA concentrations indicate that *pathway 2* was predominant. With ongoing time, *pathway 1* was gaining more and more share in DCF formation. The oxidation became rate limiting for the formation of DCF + DCF-MA. With this the concentrations of $DCFH_2$-MA and $DCFH_2$ increased (although H_2O_2 was still present). Since the oxidation was rate limiting, side reactions were largely suppressed (most of the initially added H_2O_2 was used for DCF formation and no DCF_{ox} was found). At the beginning, mainly $DCFH_2$-MA was abundant (favouring **Oxi_2**, *pathway 2*). Over time a significant concentration of $DCFH_2$ was slowly building up (slowly, on expense of $DCFH_2$-MA, see **Figure 3**), speeding up **Oxi_1** of *pathway 1*. Thereby, **Oxi_1** got more and more favoured over **Oxi_2**, therefore favouring *pathway 1* with increasing $DCFH_2$ to $DCFH_2$-MA ratio. For all three HRP concentrations, the DCF-MA

concentration remained similar at the beginning of the reacton for quite a while and then stayed

almost constant for at least 20 min (at $t \approx 260$ min, see **Figure S-21B**).

A comparison of **Oxi_1** with **Oxi_2** was made using steady-state kinetic data (see **Scheme S-1**). The DCF-MA concentration remained stable at $t = 260$ min (d[DCF-MA]/dt = 0). The comparison of **Oxi_1** and **Oxi_2** in **Scheme S-1** shows that *pathway 1* was predominant at $t = 260$. Oxidation *via* Oxi_1 was determined as faster (about 4-times) than **Oxi_2**, although [DCFH$_2$] (= 4.5 µM) was about 9-times lower than [DCFH$_2$-MA] (= 40.1 µM) at that time (see **Scheme S-1** and **Figure S-21C**). Consequently, in the following the slowly decreasing DCF-MA concentration and the stable DCF formation rate (see **Figure S-21A,B** for $t > 260$ min) showed that *pathway 1* kept being predominant for $t \approx 260$-650 min (before finally all H$_2$O$_2$ was consumed and DCF-MA hydrolysis was the last remaining DCF formation process after $t \approx 650$ min). In addition, since the DCF formation rate, dA_{460}/dt and [DCF-MA] in the steady-state (dDCF-MA/dt = 0) were all linearly dependent on [HRP] (see **Figure 7** and **Figure S-21A,B**), the same also applies for 2.5 and 7.5 nM HRP (just at altered time periods).

DCFH$_2$-MA
40.1 μM
(t = 260 min)

Hyd_2 →
d[DCFH$_2$]/dt:
$(k_{cat}/K_M) \cdot [E]_0 \cdot [S]$ =
0.0012 μM^{-1} min^{-1} · 1.0 μM · 40.1 μM =
0.048 μM min^{-1}

DCFH$_2$
4.5 μM
(t = 260 min)

Oxi_2   ④
d[DCF-MA]/dt = 0.005 μM min^{-1}
= -d[DCF-MA]/dt (**Hyd_3**)
(in steady-state)

Oxi_1   ⑤
d[DCF]/dt = 0.019 μM min^{-1}
= (d[DCF]$_{overall}$ /dt) − (d[DCF]/dt (**Hyd_3**))

DCF-MA

Hyd_3 →

DCF
5.0 μM
(t = 260 min)

②
1.2 μM
(t = 260 min)
constant,
in steady-state

③
d[DCF]/dt
= 0.005 μM min^{-1}
(calculated: $(k_{cat}/K_M) \cdot [E]_0 \cdot [S]$ =
0.0043 μM^{-1} min^{-1} · 1.0 μM · 1.2 μM)

①
d[DCF]$_{overall}$ /dt (**Hyd_3** + **Oxi_1**)
= 0.024 μM min^{-1}
(measured at t = 220-300 min)

Scheme S-1. Comparison of reaction rates, as determined for the cascade reaction run with 50 μM DCFH$_2$-DA, 9 μM H$_2$O$_2$, 1.0 μM BCA and 5.0 nM HRP at *t* = **260 min** (see **Figure S-21**). For these conditions, oxidation is rate limiting. The different hydrolysis and oxidation steps are the ones of **Scheme 2**.

The "overall" rate of formation of DCF, d[DCF]$_{overall}$/dt (as a result of **Hyd_3** + **Oxi_1**) was found to be proportional to [HRP] and was obtained from **Figure S-21A**, while the given compound concentrations (at t = 260 min) were determined by spectral fitting (**Figure S-21C**). The specificity constant, k_{cat}/K_M, for **Hyd_3** is taken from **Table S-2**. The other reaction rates were then calculated (red and blue).

❶: The overall DCF formation rate was obtained from **Figure S-21A**.

❷: Steady-state concentration of DCF-MA was from **Figure S-21C**

❸: The reaction rate for the hydrolysis of DCF-MA was calculated using [DCF-MA], [BCA] and k_{cat}/K_M. As evident from the last three entries of **Table S-2**, k_{cat}/K_M did not change significantly when DCFH$_2$ and DCFH$_2$-MA were present, even if present at higher concentration than DCF-MA.

❹: Since d[DCF-MA]/dt = 0 at *t* = **260 min**, DCF-MA formation by **Oxi_2** had to be equal to DCF-MA hydrolysis by **Hyd_3** (0.005 μM min^{-1}). Also note that the steady-state concentration of DCF-MA was linearly dependent on the amount of HRP used (**Figure S-21B**).

❺: DCF formation *via* **Oxi_1** from DCFH$_2$ could be simply calculated by subtracting the formation *via* **Hyd_3** from the "overall" formation of DCF at t = 260 min.

16. UV/vis absorption spectra and quantitative analysis of the outflow from the cascade reaction run in the glass fiber filter device with immobilised denpol-enzyme conjugates
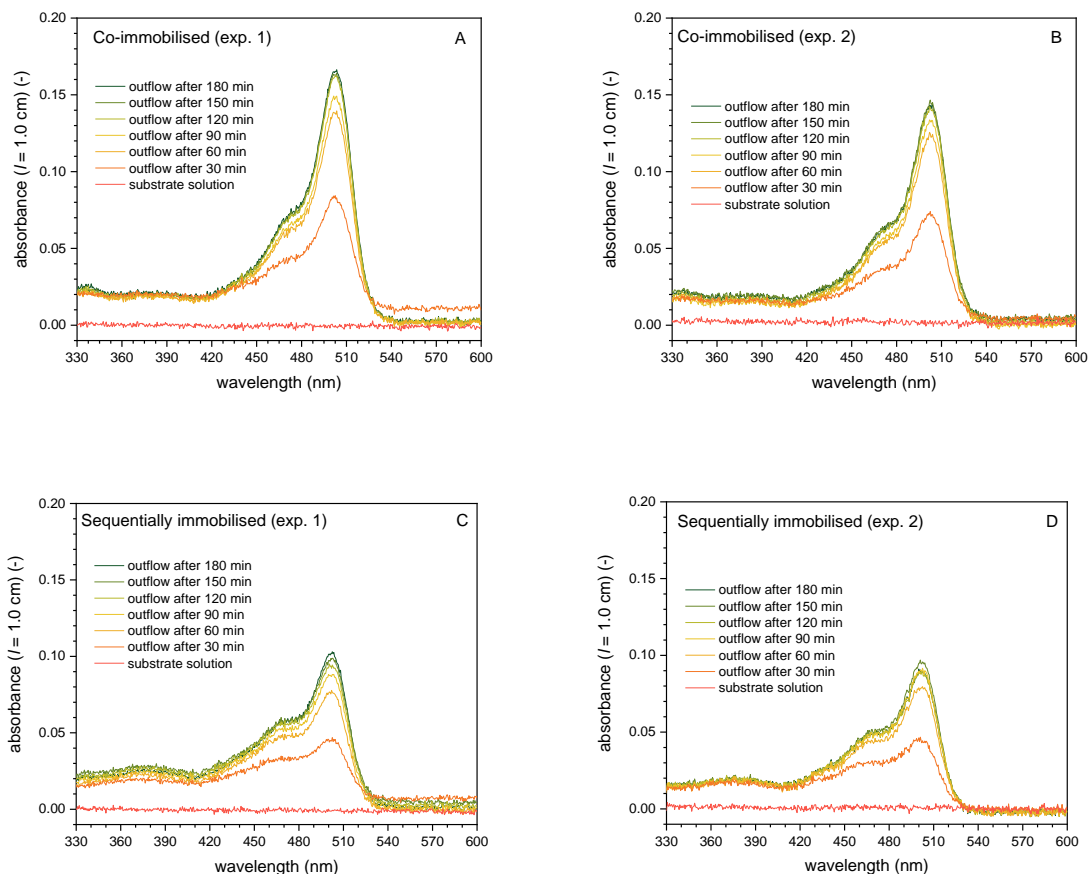

Figure S-22. UV/vis absorption spectra between λ = 330 and 600 nm of the outflow from a filter holder device consisting of two glass fiber filters with immobilised *de*-PG2$_{1000}$-BAH$_{207}$-BCA$_{152}$ and *de*-PG2$_{1000}$-BAH$_{86}$-HRP$_{90}$ (see ① in **Figure 11** and **Figure 12** ("exp.1" and "exp.2"). A substrate solution containing 50 µM DCFH$_2$-DA and 9 µM H$_2$O$_2$ was pumped through the filters and the spectra were recorded in the collected outflow after t = 30, 60, 90, 120, 150, and 180 min (t = 30 min means that the outflow was collected until 30 min; t = 60 min means, collected outflow between 30 and 60 min; etc.). Between λ = 330 and 600 nm, only oxidised species absorb (DCF, DCF-MA, and DCF$_{ox}$, see **Figure 2**). **(A)** and **(B)**: Spectra for co-immobilised conjugates (blue data points in **Figure 12**). **(C)** and **(D)**: Spectra for the sequentially immobilised conjugates (red data points in **Figure 12**).
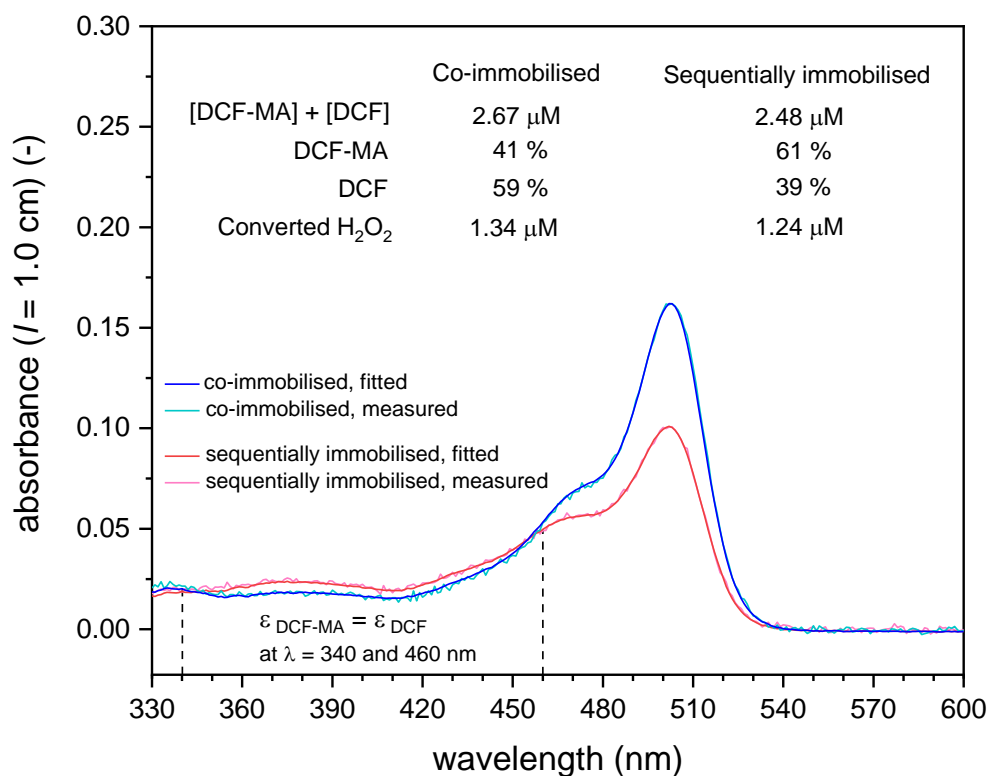
Figure S-23. UV/vis absorption spectra between λ = 330 and 600 nm of the outflow from the filter holder device for cascade reactions ① in **Figure 11** for co-immobilised (blue) and sequentially immobilsed conjugates (red), collected between t = 150 and 180 min ("exp.1", blue filled triangles and red empty triangles at t = 180 min in **Figure 12**). The measured and fitted spectra are shown with the total concentrations of DCF-MA and DCF and the relative amounts of DCF-MA and DCF present in the outflow. The fitting of the measured spectrum with the reference spectra of DCF-MA and DCF was carried out as described for the analysis of the reaction run in bulk solution (see caption of **Table S-3**).

17. References

(S1)   M. Wrona and P. Wardman, *Free Radical Biol. Med.*, 2006, **41**, 657-667.

(S2)   M. Yoshimoto, T. Schweizer, M. Rathlef, T. Pleij and P. Walde, *ACS Omega*, 2018, **3**, 10391-10405.

(S3)   C. Hou, N. Ghéczy, D. Messmer, K. Szymańska, J. Adamcik, R. Mezzenga, A. B. Jarzębski and P. Walde, *ACS Omega,* 2019, **4**, 7795-7806.

(S4)   Y. Guo, J. D. van Beek, B. Zhang, M. Colussi, P. Walde, A. Zhang, M. Kröger, A. Halperin and A. D. Schlüter, *J. Am. Chem. Soc.,* 2009, **131**, 11841-11854.

(S5)   O. Bertran, B. Zhang, A. D. Schlüter, A. Halperin, M. Kröger and C. Aleman, *RSC Adv.*, 2013, **3**, 126-140.

(S6)   H. Fischer, I. Polikarpov and A. F. Craievich, *Protein Sci.*, 2004, **13**, 2825-2828.

(S7)   S. Lindskog, *Biochim. Biophys. Acta*, 1960, **39**, 218-226.

(S8)   H. B. Dunford and J. S. Stillman, *Coord. Chem. Rev.*, 1976, **19**, 187-251.

(S9)   H. B. Dunford, *Peroxidases and Catalases: Biochemistry, Biotechnology, and Physiology*, 2nd ed., John Wiley & Sons, chapter 3, pp. 13-39 (2010).

(S10) C. Rota, C. F. Chignell and R. P. Mason, *Free Radical Biol. Med.*, 1999, **27**, 873-881.

(S11) C. Rota, Y. C. Fann and R. P. Mason, *J. Biol. Chem.,* 1999, **274**, 28161-28168.

(S12) P. Campomanes, U. Rothlisberger, M. Alfonso-Prieto and C. Rovira, *J. Am. Chem. Soc.*, 2015, 137, 11170-11178.

(S13) S. Aibara, H. Yamashita, E. Mori, M. Kato and Y. Morita, *J. Biochem.,* 1982, **92**, 531-539.

(S14) H. B. Dunford, *Peroxidases and Catalases: Biochemistry, Biotechnology, and Physiology*, 2nd ed., John Wiley & Sons, chapter 4, pp. 41-56 (2010).